Title
Freestanding complex-oxide membranes

Journal
Journal of Physics Condensed Matter, 34(38)

ISSN
0953-8984

Authors
Pesquera, David
Fernández, Abel
Khestanova, Ekaterina
et al.

Publication Date
2022-09-21

DOI
10.1088/1361-648x/ac7dd5

Peer reviewed

TOPICAL REVIEW

Freestanding complex-oxide membranes

IOP Publishing Journal of Physics: Condensed Matter
J. Phys.: Condens. Matter **34** (2022) 383001 (20pp) https://doi.org/10.1088/1361-648X/ac7dd5

Topical Review

Freestanding complex-oxide membranes

David Pesquera[1,*], Abel Fernández[2], Ekaterina Khestanova[3] and Lane W Martin[2,4]

[1] Catalan Institute of Nanoscience and Nanotechnology (ICN2), CSIC and BIST Campus UAB, Bellaterra, Barcelona 08193, Spain
[2] Department of Materials Science and Engineering, University of California, Berkeley, CA 94720, United States of America
[3] ICFO-Institut de Ciencies Fotoniques, 08860 Castelldefels (Barcelona), Spain
[4] Materials Sciences Division, Lawrence Berkeley National Laboratory, Berkeley, CA 94720, United States of America

E-mail: david.pesquera@icn2.cat

Received 22 April 2022, revised 14 June 2022
Accepted for publication 1 July 2022
Published 18 July 2022

Abstract

Complex oxides show a vast range of functional responses, unparalleled within the inorganic solids realm, making them promising materials for applications as varied as next-generation field-effect transistors, spintronic devices, electro-optic modulators, pyroelectric detectors, or oxygen reduction catalysts. Their stability in ambient conditions, chemical versatility, and large susceptibility to minute structural and electronic modifications make them ideal subjects of study to discover emergent phenomena and to generate novel functionalities for next-generation devices. Recent advances in the synthesis of single-crystal, freestanding complex oxide membranes provide an unprecedented opportunity to study these materials in a nearly-ideal system (e.g. free of mechanical/thermal interaction with substrates) as well as expanding the range of tools for tweaking their order parameters (i.e. (anti-)ferromagnetic, (anti-)ferroelectric, ferroelastic), and increasing the possibility of achieving novel heterointegration approaches (including interfacing dissimilar materials) by avoiding the chemical, structural, or thermal constraints in synthesis processes. Here, we review the recent developments in the fabrication and characterization of complex-oxide membranes and discuss their potential for unraveling novel physicochemical phenomena at the nanoscale and for further exploiting their functionalities in technologically relevant devices.

Keywords: freestanding, membranes, complex oxides

(Some figures may appear in colour only in the online journal)

1. Single-crystal nanomembranes: a novel playground for oxide physics

Launched by the graphene revolution, the field of two-dimensional (2D) atomic crystals—including mono- and few-layer transition metal dichalchogenides (TMD's), hexagonal boron nitride (hBN), metal halides, and many others [1–4]—has become one of the most productive areas of research in terms of novel physics and device concepts with potential near-future applications within the condensed matter physics community [5]. When isolated as 2D crystals, these materials can exhibit exceptional electronic [6], optoelectronic [7], mechanical [8], and topological [9] properties. Moreover, 2D membranes allow for mechanical manipulation via multiple approaches [10], and their versatile stacking mediated by

* Author to whom any correspondence should be addressed.

van-der-Waals interactions enables their facile integration with existing technological platforms. More recently, the possibility to control the misorientation between layers in artificially assembled heterostructures has enabled the advent of *twistronics* approaches—a new fabrication concept to tune electronic interactions and create emergent correlated behaviors such as superconductivity, ferroelectricity, or magnetism in graphene [11–13], hBN [14] or TMD's [15].

On the other hand, transition-metal oxides (TMOs)—in particular the ABO_3 perovskite materials—can exhibit a much richer range of functionalities (in part because many fall into the category of strongly correlated materials), including: Mott insulating behavior and metal-to-insulator transitions [16], multiferroicity [17], ionic conduction [18], colossal magnetoresistance [19], confined superconductivity [20], or large oxygen catalytic activity [21], to name just a few. This wide variety of properties arises from the electronic structure governed by strongly localized and highly anisotropic *d*-electron bands from the transition-metal cations and their hybridization with the oxygen *p* orbitals, combined with a highly versatile perovskite crystal structure, where a number of symmetry distortions at the unit-cell level (such as displaced cations or tilted-oxygen octahedra) can create local dipoles, tune the charge distribution between metal and oxygen ions, or modify the magnetic interactions of unpaired electrons. As a result of this complexity, perovskite oxides show a vast array of competing (and sometimes coexisting) phases and phenomena, where the ground state is largely dependent on chemical doping, temperature, magnetic field, or applied pressure/stress. For relevant literature on the physics of TMOs, for which this review is not intended to provide in depth coverage, the reader is referred to other sources [22–24].

Such complexity in perovskite oxides has complicated their study, both experimentally and theoretically. One traditional materials-science approach to address this has been to work to be able to better control and understand the functional properties of oxides by synthesizing nanoscale films and heterostructures on compatible single-crystal oxide substrates, whereby the chemistry and structure can be precisely engineered at the atomic level [25–27]. As long as the lattice mismatch between the film and the substrate is small (typically less than a few percent) and a certain thickness threshold is not surpassed (typically <100 nm), single crystalline films with a low density of dislocations can be produced. This not only allows for the study of complex oxides in a simplified system, but also for the creation of new artificial materials via epitaxial strain engineering [28] and heterostructuring [29], thus leading to new functionalities promoted by interface design [30, 31], quantum confinement [32, 33], surface control [34–36], or stabilization of different structures [37, 38], electronic phases [39–41], and domain patterns [42].

Whereas epitaxial systems are ideal to control structure-property relationships, the strong chemical bonding with the substrate imposes severe mechanical constraints on the films. On the one hand, the elastic deformations that one can induce in the films is limited to the planar strains induced by the epitaxy on the available and compatible substrates. On the other hand, substrates govern the elastic response of the system, limiting the functional response of the films associated to structural changes upon application of external stimuli, such as piezoelectric/magnetostrictive deformations, ferroelastic domain motion during polarization switching in ferroelectrics (FEs) [43], or strain-mediated magnetoelectric effects in multiferroic heterostructures [44]. Releasing epitaxial oxide films from the growth substrate is, therefore, an alluring opportunity to expand the knowledge of these materials by exploring their intrinsic response in a 2D isolated system, to envision new strategies for mechanical manipulation, or to produce nanoscale devices made from highly crystalline materials.

Epitaxial oxides are also promising material systems to integrate on transistor devices with higher speed and lower voltage/power operation. To make possible a new generation of oxide electronic devices, however, a few bottlenecks need to be overcome, the main one being the compatibility with the prevailing complementary metal-oxide semiconductor (CMOS) technology. Possibilities for coupling or interfacing dissimilar materials (e.g. integrating oxides with traditional group IV or III–V semiconductors) are also strongly limited by the stringent restrictions of the synthesis processes (i.e. epitaxial relationships, chemical compatibility, thermal mismatch, etc). Considerable effort has been put into establishing procedures for direct epitaxial growth of oxide films on silicon via physical and chemical methods [45], aiming to make oxide growth conditions (i.e. high temperatures and oxidizing environments) compatible with silicon. Non-standard growth methodologies and appropriate buffer/passivation layers have been developed to suppress SiO_2 formation or mitigate the excessive epitaxial and thermal stress imposed on the films [46, 47]. Interfacial charge-trapping states and band offsets are, however, difficult to control and deteriorate the performance of high-k dielectrics (such as $SrTiO_3$) by reducing channel mobility, or prevent the proper function of FE field effect transistors (FETs) using FE gate materials (such as $BaTiO_3$), due to charge screening of the polarization [48].

The integration of oxides on flexible platforms is another stop on the path towards oxide electronics facing similar challenges, since polymer substrates and high growth temperatures used for crystallization are incompatible. Oxide perovskite FEs are preferred over flexible organic FEs such as polyvinylidene difluoride because of their higher polarization and switching speed, and lower coercive fields. Epitaxial synthesis on layered muscovite substrates offer a solution for integrating oxides on flexible platforms [49, 50] and for testing their performance under bending conditions, but polymer platforms are still the preferred choice for flexible device fabrication at the commercial scale.

'Bond-free' integration schemes used in van-der-Waals heterostructures, in turn, would allow one to overcome the limitations related to incompatible chemistries, high-temperature synthesis, and/or structural matching, thus enabling a wider range of materials combinations simply coupled via intermolecular interactions through clean, flat interfaces [51]. This strategy has boosted the development of numerous (opto-)electronic devices in which one or more building blocks are assembled onto a semiconductor or flexible platform

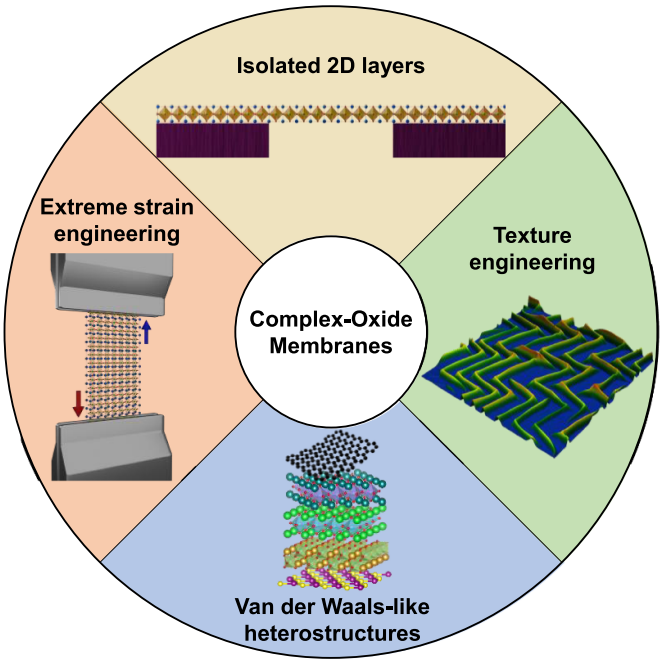

Figure 1. Novel possibilities offered by the synthesis of complex-oxide membranes.

[52–54]. The incorporation of such fabrication processes to the family of complex oxides is poised to provide new and valuable opportunities in manipulating structures, exploring the physics of freestanding films, and integrating functionalities in novel design concepts (figure 1). The complex-oxides community is starting to realize this potential and, in the last five-year period, multiple approaches for the synthesis of substrate-isolated and purely freestanding oxide nanomembranes have been developed. In this short period of time, surprising results such as the large strain tunability of freestanding oxides [55, 56] with deformations well beyond that which is achievable in bulk or epitaxial films, the stability of just few-layer-thick freestanding membranes [57, 58], and the demonstration of high-performance flexible devices made from single-crystal oxides [59, 60] have promoted increased interest in substrate-release strategies for oxide perovskites, mostly focused on FE materials due to the wide array of possibilities in lattice control of properties [61] and significant interest in CMOS [62] and flexible [63] integration. While still in its infancy, the field of 'oxide-membrane engineering' has already produced significant fruits and laid the foundation for new groundbreaking studies to come.

Here, we review the progress in the field of single-crystal, complex-oxide nanomembranes, including recapping a number of milestones and unforeseen opportunities offered by the application of this processing approach to such multifunctional materials. In section 2, we summarize the different synthesis/fabrication approaches explored thus far, highlighting the achievements and challenges of these processing techniques applied to oxides. In section 3, we discuss the most relevant breakthroughs on approaching 2D limits in oxide membranes. In section 4, we describe novel strategies for strain control of properties of freestanding membranes beyond what can be achieved in epitaxial films. In section 5, we comment on the microstructural and functional effects found in the single-crystal membranes under bending/strain gradient conditions and their prospective use in nanomechanical systems. In section 6, we review the progress on complex-oxide integration of devices on silicon and flexible platforms using membrane transfer techniques, and the potential for improved performance of these devices with respect to epitaxial systems. Finally, in section 7, we overview possible future avenues for the exploitation of this technology for new measurement and actuation approaches, stabilization of new properties or electronic phases, and for the combination of materials so far unachievable via standard methods.

2. Epitaxial lift-off and van der Waals assembly

The development of freestanding membranes of complex oxides has been strongly motivated by the diversity of novel physics and phenomena observed in van der Waals materials such as graphene, hBN, and TMDs. Yet, unlike van der Waals materials, the strong metal-oxygen orbital hybridization that gives rise to the rich physics of complex oxides also precludes the simple separation of individual atomic layers, or of deposited thin films from their substrates in the vast majority of compositions. As the approaches developed over the last five years have matured, the variety of materials that can now be synthesized as completely freestanding nanomembranes has grown. Following the blueprint set forth by researchers studying graphene, atomically thin nanosheets were created by identifying layered oxide structures where, similar to graphene and other van der Waals materials, the interlayer bonding was relatively weak, and individual layers could be mechanically separated. Other methods aimed to leverage the ease of exfoliating graphene as a separation layer, to allow for detachment of a deposited thin film from its substrate. Now, chemical etching of a suitable buffer layer has allowed for the application of well-developed epitaxial synthesis, device fabrication, and characterization techniques to be applied to wide array of oxide compositions with various functionalities. Here, we review the development of synthesis and fabrication techniques for production of freestanding-oxide membranes.

2.1. Exfoliable oxides

The desire to isolate atomically thin layers of oxides is not new. For several decades, chemical methods involving intercalation and subsequent separation of atomic layers of a number of oxide compositions were used to isolate monolayers from bulk crystals [64, 65]. These methods resulted in slurries of flakes with varying thickness and relatively small areas. Such methods have been used to produce a number of transition metal oxides as nanosheets limited to a single layer of the parent material, including a number of titanium- and manganese-based oxides [66], as well as more complex layered perovskites and related structures, including, $Bi_2SrTa_2O_9$ [67], $Ca_2Nb_3O_{10}$ [68], and $Sr_2Nb_3O_{10}$ [69] albeit with small areas on the order of tens-to-hundreds of

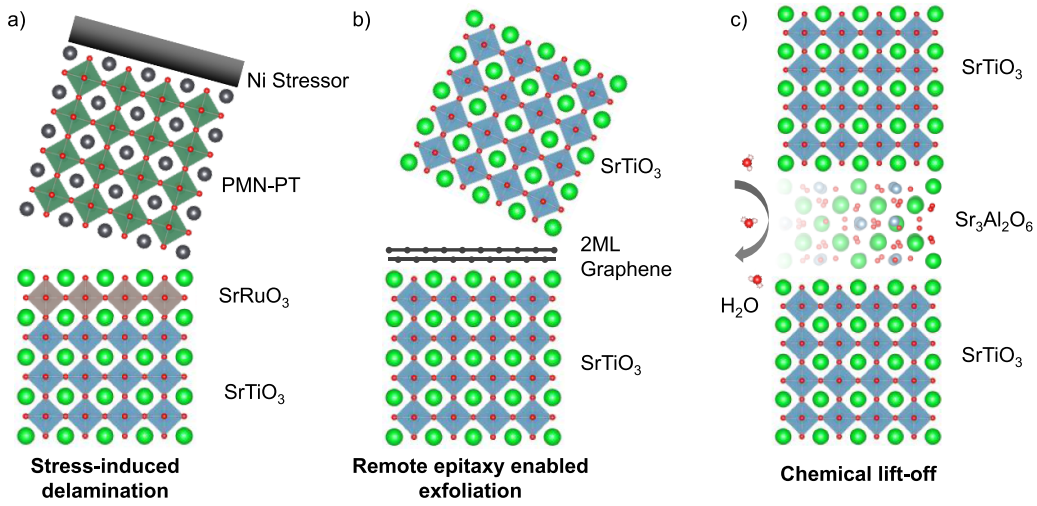

Figure 2. Representative methods developed recently to fabricate freestanding membranes of complex oxides, including: (a) mechanical release, via stress-induced breaking of weakly bonded interfaces; (b) exfoliation enabled via intercalated graphene; and (c) chemical etching of a sacrificial layer. (a,b) reproduced from [79], with permission from Springer Nature.

square microns. Nevertheless, such monolayers have been used to create multilayer structures composed of alternating layers of monolayer oxides. These multilayer structures rely on self-assembly of the nanosheets during sequential dipping of the substrate in respective colloidal suspensions, limiting the deterministic manipulation of single sheets.

Mechanical exfoliation of bulk crystals on the other hand, has been used for years to cleave crystals of layered oxides in ultrahigh vacuum to expose clean surfaces for measurements where surface contamination is impermissible (e.g. in angle-resolved photoemission spectroscopy and scanning tunneling microscopy) [70, 71]. More recently, mechanical exfoliation has been shown to allow for the isolation of monolayer sheets. Rather than rely on chemical intercalation, mechanical exfoliation involves repeated splitting of a bulk crystal with weak interlayer interactions until a monolayer is achieved. This method is simple and straightforward to implement, only requiring a surface which flakes can stick to, and has been compared to 'drawing by chalk on a blackboard' [72]. While the relative simplicity and low startup-costs for producing samples has contributed to the rapid expansion of the field of 2D-materials research, the technique also relies on the serendipitous delamination of monolayers, which are typically found as a minority occurrence amongst flakes of many different thicknesses. Identifying monolayer flakes is performed optically, either with visual inspection of the contrast created by a monolayer on a substrate (which has the added complication of being substrate dependent), or via layer-dependent signatures in Raman spectra [73]. As the field has expanded, numerous methods utilizing various support layers to increase flake size and yield have been studied, including, for example, use of gold surfaces for better adhesion and large-area monolayers [74], as well as a variety of thermoplastic polymers for the controlled transfer of monolayers for device fabrication.

While researchers studying graphene, h-BN, and TMDs have rapidly improved the ability to produce, transfer and fabricate monolayers from bulk crystals, mechanical exfoliation of oxides remains less successful. In the seminal work demonstrating isolation of monolayer graphene and other van der Waals materials [72], a layered superconducting oxide, $Bi_2Sr_2CaCu_2O_x$ was also exfoliated down to a single layer, although no superconductivity was observed in the monolayer samples. Yet, since then, there remains only a few studies on the exfoliation of layered oxides [73, 75, 76]. Nevertheless, work continues to expand the available exfoliable oxides, including development of synthesis techniques to create novel layered oxide structures. For example, recent work found that controlled oxidation of metal surfaces resulted in a novel, layered hexagonal structures of a number of transition-metal, lanthanide, and metalloid binary oxides which could be exfoliated to monolayer thicknesses [77].

In some cases, oxide films can be mechanically removed from the substrate via spalling, rather than exfoliation. Here, a stressor layer is deposited on the film to be released, applying large tensile strain and driving propagation of a crack parallel to the film-substrate interface. A flexible handle layer applied to the stressor layer then allows for peeling and transfer of the delaminated film. This technique, originally studied for release of semiconductor layers [78], has only recently been applied to complex oxides. For example, 500 nm thick $PbMg_{1/3}Nb_{2/3}O_3$–$PbTiO_3$ (PMN-PT) films have been mechanically removed from $SrRuO_3$-buffered $SrTiO_3$, where a 5 μm thick nickel stressor layer induced crack-propagation precisely at the PMN-PT/$SrRuO_3$ interface [79] (figure 2(a)). Stress-induced spalling was also observed in self-formed freestanding $LaAlO_3/SrTiO_3$ micro-membranes [80]. There, the large lattice mismatch between the deposited $LaAlO_3$ layer and the $SrTiO_3$ substrate drives crack propagation below the surface of the $SrTiO_3$. This spontaneous cracking resulted in formation of curved, freestanding bilayers with areas on the order of tens-to-hundreds of square microns that maintain the metallic nature of the 2D electron gas at the $LaAlO_3/SrTiO_3$ interface. The curvature of the freestanding membranes, formed due to the asymmetric lattice parameters

of the bilayers, results in large strain gradients (on the order of 1 μm^{-1}). Further studies demonstrated a pre-patterning approach that allowed for control of the size of the spalled micromembranes [81]. Despite these reports, however, mechanical approaches to release complex-oxide films are still limited to a few particular compositions.

2.2. Graphene intercalation

Achieving 2D crystals of oxide materials that do not inherently possess layered structures for easy delamination, like the family of perovskites, has required more creative approaches. Advances in epitaxial deposition of oxide-thin films allows for routine synthesis of ultrathin crystals with atomically precise thicknesses. Critical to the crystalline quality of these films is the availability of an appropriate substrate that is isostructural and has relatively small lattice mismatch with the deposited epilayer. The strong covalent bonding of such epitaxial films, however, prevents mechanical exfoliation of the deposited film from the substrate. One approach to enabling exfoliation has been to prevent the covalent bonding of the deposited film to the underlying substrate, utilizing a graphene buffer layer [82]. Here, an epitaxial graphene layer is deposited on the substrate prior to thin-film deposition, providing a weak, van der Waals-bonded layer between the film and substrate. Importantly, the 2D graphene layer is thin enough to allow the charge-density of the substrate surface to penetrate, providing a surface potential for deposited adatoms to align epitaxially with the underlying substrate [83]. This so-called remote epitaxy thus provides a method for epitaxial deposition of arbitrary covalently bonded materials, while maintaining an exfoliable, van der Waals layer.

This technique was first employed to synthesize epitaxial, single-crystalline GaN films which could be exfoliated and transferred to arbitrary substrates [84]. Since this initial work, the approach has been expanded to oxides, including spinels (e.g. $CoFe_2O_4$), garnets (e.g. $Y_3Fe_5O_{12}$), and perovskites (e.g. $SrTiO_3$) [79] (figure 2(b)). This remote epitaxy has enabled the fabrication of epitaxial heterostructures of dissimilar materials, as in the case of the heterogeneous integration of epitaxial films of ferromagnetic $CoFe_2O_4$ exfoliated and transferred to PMN-PT films to realize a composite multiferroic [79].

2.3. Chemical lift-off

Despite advances in mechanical approaches, chemical approaches have become the most widespread used to produce membranes today. In this case, a sacrificial layer which can be dissolved in an appropriate etchant, is epitaxially grown between the substrate and film. Such methods have been used for several decades for epitaxial lift-off of semiconductor devices, with sacrificial layers including AlAs [85] and SiO_2 [86]. For example, this is common practice in the fabrication of solar-cell arrays, where transfer of thin film solar cells to a back reflector layer has led to increased efficiencies [87].

There is increasing attention on using complex oxide sacrificial buffer layers to allow for the release of large area films from their substrates. The benefit of using a complex-oxide buffer layer, as opposed to the graphene buffer layer described before, is the ease with which it can be introduced to already existing oxide-deposition techniques, for which synthesis of multilayer heterostructures with atomic precision is already well developed. The sacrificial layer has a few key requirements to allow for release of high-quality, epitaxial oxide films. First, an appropriately selective etchant must be available such that the film to be released remains undamaged during the etch. Second, the sacrificial layer should provide an adequate template for subsequent deposition of the desired oxide film. This includes both an appropriate lattice parameter, and ideally the same structure, such that the full heterostructure can be coherently strained, providing for the deposition of high-quality, single-crystalline films. The earliest reports of freestanding complex oxide nanomembranes, in fact, exploited already existing etch processes developed for the termination-control of $SrTiO_3$ substrates. In that work, the well-known buffered-HF etch of $SrTiO_3$, which is typically used to selectively remove the SrO surface layer and create TiO_2-terminated substrates, was used to separate large area $SrRuO_3$ membranes [88]. In some cases, the small cross-section and slow etch rate of SrO, however, required the fabrication of films with etchant access holes, limiting the continuous area that could be released as a nanomembrane [89]. Moreover, while $SrTiO_3$ is a widely used substrate for oxide epitaxy, promising a wide range of materials which could potentially be released as nanomembranes, the buffered-HF etch limits this approach to materials which can withstand this particularly aggressive etchant.

With a growing need for more versatile sacrificial layers with more benign etchants, researchers developed approaches for the epitaxial deposition of $Sr_3Al_2O_6$, a hygroscopic complex oxide with a similar cation sublattice to prototypical perovskites [90]. Layer-by-layer epitaxy on $SrTiO_3$ substrates and subsequent deposition of perovskite layers on the $Sr_3Al_2O_6$ buffer layer was ultimately demonstrated, and, due to the strongly hygroscopic nature of the $Sr_3Al_2O_6$, subsequent etching can be performed in water, expanding the variety of films that can be released from the substrate (figure 2(c)). While $Sr_3Al_2O_6$ conveniently possesses low lattice mismatch with $SrTiO_3$, calcium- or barium-substitution for strontium can be used to continuously tune the lattice parameter from 3.82 Å for $Ca_3Al_2O_6$ to 4.13 Å for $Ba_3Al_2O_6$, providing a water-soluble sacrificial layer that covers a wide range of commercially available perovskite-oxide substrates [55]. Using these sacrificial layers, a number of compositions, including $PbTiO_3$ [91], ultrathin $BiFeO_3$ and $SrTiO_3$ [58], $La_{0.67}Sr_{0.33}MnO_3$ [90] with different orientations [92], $La_{0.7}Ca_{0.3}MnO_3$ [55], $BaSnO_3$ [93], $BiMnO_3$ [94], VO_2 [95], and $YBa_2Cu_3O_{7-\delta}$ [96] have been released as freestanding membranes and transferred to a number of substrates. Additionally, complex heterostructures including superlattices [90] and microfabricated devices (e.g. FE tunnel junctions [97]) have also been released and transferred. For the most part, synthesis of epitaxial $Sr_3Al_2O_6$ films has been carried out by molecular=beam epitaxy or pulsed-laser deposition, but groups are also now working towards less costly means of synthesis. For example, epitaxial $Sr_3Al_2O_6$ films have recently been synthesized on

$SrTiO_3$ substrates via chemical solution deposition, utilizing both metal-organic and metal nitrate precursor solutions, and used to release free-standing Al_2O_3 membranes [98]. While promising, the high reactivity of $Sr_3Al_2O_6$ also leads to difficulty in synthesis and poor stability in ambient air, with reported degradation of the exposed $Sr_3Al_2O_6$ surface occurring in a matter of minutes [99] and even degradation of the source target to a point that it can no longer be used unless carefully stored.

Another common sacrificial layer that has been adopted is using compositions in the $La_{1-x}Sr_xMnO_3$ system [100–102], for which epitaxial deposition is already well established. In this case, etching proceeds via reduction of the manganese-site in acidic solution, often with a potassium iodide as a reduction agent. While limiting the available layers for release to those that can withstand the acidic, reducing etchant, many FE oxides, for example, have proven to be resistant to this particular etchant. In particular, it has been shown that deposition of $La_{1-x}Sr_xMnO_3$ via pulsed-laser deposition in low partial pressures of oxygen can drive high defect densities which allow coherent deposition of films to commercially available oxide substrates from $LaAlO_3$ (pseudocubic lattice parameter of 3.78 Å) to $NdScO_3$ (4.00 Å) [103]. As such, this has enabled the deposition of epitaxial films of large lattice-parameter FEs including $BaTiO_3$ and $0.68PbMg_{1/3}Nb_{2/3}O_3$–$0.32PbTiO_3$ [102], in addition to $PbZr_{0.2}Ti_{0.8}O_3$ (PZT) [101] and $BiFeO_3$ [104].

While the above sacrificial layers have been of predominant use for the release of complex-oxide perovskites, alternative sacrificial layers have been used. BaO, for example, has been used as a water-soluble sacrificial layer for the release of $BaTiO_3/SrTiO_3$ heterostructures from $SrTiO_3$ substrates [105]. Although strontium-doping of BaO promises a water-soluble sacrificial layer with a tunable lattice parameter, its necessary to deposit a perovskite buffer layer on the (Ba,Sr)O buffer layer to re-establish the perovskite structure before depositing the desired film for release. Release of epitaxial films with non-perovskite structures further requires new sacrificial layers with alternative structures. For example, epitaxial NaCl sacrificial layers have been used for the release of nano-structured WO_3 and Sn-doped In_2O_3 [106]. Freestanding VO_2 membranes have been released using a ZnO sacrificial layer deposited on Al_2O_3 substrates resulting in millimeter-sized films of VO_2 which could be transferred to flexible substrates [107]. The symmetry mismatch of the VO_2 and ZnO layers, however, resulted in the formation of a multivariant VO_2 film. Achieving freestanding, single-variant VO_2 films required a multi-step deposition and release process wherein VO_2 was initially used as a sacrificial layer to release a rutile TiO_2 layer [108]. The freestanding TiO_2 layer was subsequently used to template a deposited VO_2 layer, providing a method for synthesizing freestanding VO_2/TiO_2 heterostructures without exposing the VO_2 to the etch process. Other recent examples of non-perovskite sacrificial layers include the release of spinel $CoFe_2O_4$ membranes utilizing MgO as a sacrificial layer and subsequent etching in H_3SO_4 solution [109]. The chemical etch of an epitaxial sacrificial layer has thus provided new routes towards fabricating freestanding membranes of numerous oxide compositions.

2.4. Transfer methods: opportunities and challenges

For complex oxides in particular, the transfer process represents the largest hurdle for obtaining large-area, crack-free membranes. The brittle nature of complex-oxide structures requires careful consideration of the stresses occurring during the etch and transfer process. As discussed above, choice of a lattice-matched sacrificial layer, which allows for growth of coherent films with lower internal stress. This was demonstrated, for example, in the release of $Ba_{1-x}La_xSnO_3$, which has a relatively large lattice parameter ($a = 4.116$ Å) [93]. Using $Sr_3Al_2O_6$, possessing a lattice mismatch with $BaSnO_3$ of 5.4%, resulted in heavily wrinkled and cracked membranes upon release, attributed to the internal stresses in the partially-relaxed $BaSnO_3$ film. Instead, using $Ba_3Al_2O_6$ ($a_{pc} = 4.125$ Å) as a sacrificial layer provided a smaller lattice mismatch of 0.21%, resulting in large-area, crack-free membranes. Internal stresses in the polymer support can also induce wrinkling and cracking during the etch process. This observation has been exploited to drive formation of periodic wrinkle-patterns in released $BaTiO_3$ membranes [110]. A pre-stressed (poly)dimethylsiloxane (PDMS) layer was used to support the $BaTiO_3$ during etching of the sacrificial layer, and upon release of the polymer strain, the $BaTiO_3$ formed a periodic array of striped, zig-zag, or mosaic wrinkles, controlled by the magnitude and direction of the initial polymer stress.

Once films are released from the substrate, a number of transfer and fabrication methods are available for manipulation of the freestanding membrane [111]. Achieving large-area complex-oxide membranes has been facilitated through the use of a polymer support layer during the etching process, which can then be used as a handle for the transfer to different substrates. Borrowing from the approaches that are now commonplace for transfer of semiconducting device arrays and 2D materials, a PDMS rubber stamp is commonly used to pick up and stamp freestanding-oxide membranes. Using only the PDMS stamp, the transfer process can be carried out by relying on stronger adhesion between the membranes and the receiving substrate as compared to the adhesion between the membrane and PDMS [112]. Leveraging the viscoelasticity of the PDMS, studies have demonstrated selective pick-up and stamping of device arrays based on the contact speed (e.g. rapid peeling of the PDMS layer promotes adhesion of freestanding membrane to the PDMS, while the slow peeling of the PDMS post-transfer promotes adhesion to the receiving substrates). Alternative polymers, for example (poly)methyl-methacrylate, can be used to support and transfer membranes to a receiving substrate, and the polymer support can subsequently be dissolved in acetone or other organic solvent, leaving the membrane adhered to the receiving substrate. Yet this can be too aggressive for brittle oxide membranes, and use of thermoplastic polymer supports has seen increasing use in the oxide community. One increasingly popular approach in both the 2D and oxide communities is to use

a PDMS stamp coated by a thin layer of a thermoplastic polymer like polypropylene carbonate (PPC) or polycaprolactone [55, 102, 113, 114]. At low temperatures, the thermoplastic polymer is rigid and provides strong adhesion and mechanical support to the released membrane, but upon heating undergoes a rapid transition, becoming softer and more pliable. Using PPC, which has a glass transition near 40 °C allows for controlled pick-up and release of different freestanding membranes, requiring only moderate heating. PPC can additionally be removed by dissolution in acetone or thermal decomposition upon heating above 250 °C.

Outside of the successful release of crack-free films is the subsequent transfer of the film to the desired substrate, and beyond, the controlled interfacing of multiple released complex-oxide membranes. Assembly of heterostructures from different complex-oxide membranes provides new routes for integration of materials that would be impossible with conventional epitaxy [51]. Heterostructures of dissimilar complex oxides, like garnets and perovskites, can be difficult to accomplish via *in situ* epitaxial deposition since the growth of high-quality films of one structure precludes use of a substrate with the appropriate structure and lattice parameters for the second layer, or, at the very least, dramatically limits the number of compositions where this is possible. Similarly, heterostructures of films with very different optimal deposition conditions, for example, growth temperature or gas atmosphere, is limited by the ability to deposit these materials simultaneously without sacrificing the quality. On the other hand, release and transfer of high-quality epitaxial films of arbitrary structure and chemistry can be achieved. Additionally, creating heterostructures where two crystals are interfaced with an arbitrary angle is nearly impossible with conventional epitaxial approaches. Yet novel physical phenomena, like superconductivity in 'magic-angle' graphene, are driving growing interest in the field of 2D materials, and particularly for use in new twistronics devices [11]. Fabrication of such heterostructures has driven development of membrane-transfer systems that integrate mechanical manipulation of the polymer stamp with optical probes to deterministically control the orientation between different layers [115, 116]. Such systems offer the benefit of x–y–z and angle positioning, as well as controlled stamping and peeling speeds and forces and controlled stamping angle to modulate the contact-front speed [117]. These methods have been used to transfer crack-free, millimeter-sized membranes, as well as pre-fabricated device arrays, to arbitrary substrates, including silicon and flexible polyethylene terephthalate (PET) substrates.

3. Two-dimensional perovskites

Once the epitaxial oxide films are released from the substrates, the resulting freestanding membranes display two surfaces and in a purely 2D crystal, the whole sample is only surface. The study of surfaces in TMOs is crucial to understand their oxygen reactivity, relevant for catalytic processes related to oxygen-reduction reactions [118, 119], but also to unveil emergent surface properties that radically differ from those of the bulk material [120]. Considering the strong effect of crystal field and atomic environment alterations on the electronic configuration of these materials, such a drastic rupture of inversion symmetry in a freestanding 2D membrane necessarily leads to materials with strongly modified properties dependent on dangling bonds and surface electronic reconstructions. Surface-sensitive probes have been traditionally used to study oxide surfaces in bulk crystals or epitaxial films, however complete separation between the surface and the rest of the system (bulk material or substrate) is not possible in general. The synthesis of 2D crystals of TMOs is thus ideal to study isolated surfaces, understand their microscopic phenomena, and reveal new emergent phases.

3.1. Stability of monolayer perovskite membranes

One question that researchers have been working to address is whether a purely 2D crystal of a perovskite (i.e. 1 unit cell thick) is stable at finite temperatures. In graphene and related van-der-Waals exfoliated 2D crystals, thermal fluctuations can easily move the atoms outside equilibrium in the out-of-plane direction due to the lack of neighboring atoms, destroying the crystalline order at finite temperatures; however, the membranes spontaneously produce height fluctuations (ripples), causing the stiffening of the acoustic vibrational modes and the stabilization of the lattice [121, 122]. Researchers have studied [57] the crystalline order of the archetypical TMO $SrTiO_3$ by synthesizing freestanding membranes from single crystal epitaxial films (grown by pulsed-laser deposition) with thicknesses between 1 and 10 unit cells. Transmission electron microscopy (TEM) observations revealed relatively long-range structural order until the thickness reached 5 unit cells, below which an exponential decrease of the crystalline coherence length was observed with further thickness reduction (figure 3(a)). Interestingly, the authors also discovered a thickness trend for the dislocation density in the membranes which was relatively constant for membranes 6–10 unit cells thick, but increased drastically for membranes <5 unit cells thick; evidencing that crystalline order is maintained via formation of dislocation pairs and defining a critical thickness below which the dislocations propagate and the order is lost. This study revealed that the production of 2D crystals of oxide perovskites (and other ionic compounds) may be more challenging than those of van-der-Waals materials, the main difference being the energy released by the bond breaking in the membrane fabrication process. In the case of materials with high bonding anisotropy (such as exfoliable layered compounds), the monolayer limit is reachable since the perturbation induced by the bond breaking is insignificant; however, in the case of ionic compounds, the high energy released during the epitaxial lift-off process may destroy the crystalline order at room temperature below a certain film thickness. This critical limit was, however, later overcome [58] when researchers reported TEM observations of $SrTiO_3$ freestanding membranes made from single crystal epitaxial films grown by molecular-beam epitaxy. In this case, the diffraction patterns of the membranes show single-crystal order down to single unit cell and the membranes display

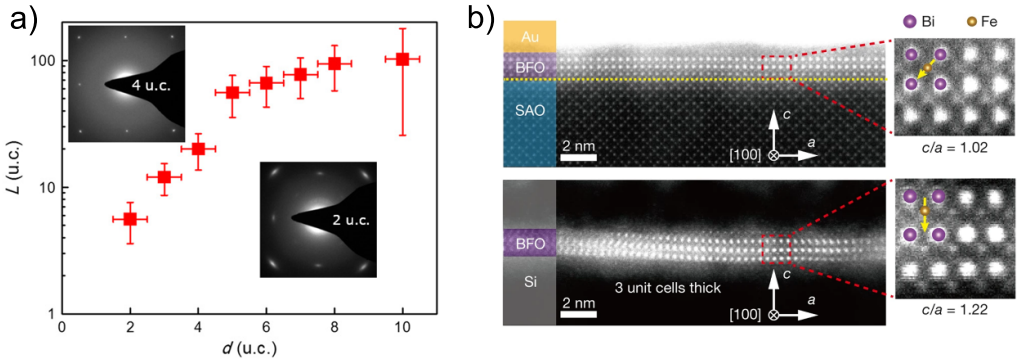

Figure 3. (a) Crystalline coherence length L as a function of thickness for $SrTiO_3$ suspended membranes. The insets are diffraction patterns obtained in TEM. From [57]. Reprinted with permission from AAAS. (b) Cross-sectional HAADF images of a 3-unit-cell-thick $BiFeO_3$ film before (top) and after (bottom) epitaxial liftoff. The insets show the transformation from rhombohedral to tetragonal symmetry and the corresponding polar displacement. Reproduced from [58], with permission from Springer Nature.

considerable roughening, which may indicate a stabilization mechanism free of dislocations similar to the ripples observed in graphene. Further work is therefore needed to clarify the experimental conditions under which crystalline order can be preserved in (few-)mono-layer oxide membranes. Other synthesis approaches, probably involving weakly bonded interfaces [79] should also be explored as alternative methods for the synthesis of these 2D membranes.

3.2. Emerging properties in monolayer membranes

The successful synthesis of oxide perovskite monolayers also opens the way for the exploration of intrinsic critical thickness for ferroic order. For example, the existence of a fundamental thickness limit for ferroelectricity is a long-standing debate. Whereas first-principles calculations suggested an enhanced polarization in few-unit-cell-thick $PbTiO_3$ [123], more realistic simulations considering electrode interfaces reveal a lower limit for the ferroelectric instability of ∼6 unit cells in $BaTiO_3$ [124], in agreement with later experimental reports [125] and with the presence of a depolarization field originated from incomplete charge screening at the electrode-FE interfaces, suppressing the polarization, while extrinsic factors like epitaxial strain or ionic polarization induced at electrode interfaces can reduce or even suppress this critical thickness [126, 127]. Freestanding single-crystal membranes allow for the study of the inherent properties of these materials and their intrinsic mechanisms for structural, electronic, and polar reconstructions in the bidimensional limit. With this scope, researchers [58] obtained freestanding single-crystal membranes of $BiFeO_3$ with thicknesses down to 2 unit cells. Cross-sectional high angle annular dark field TEM images revealed a dimensionality-driven phase transition from rhombohedral bulk-like structure at larger thicknesses to a giant tetragonal distortion below 3-unit-cells thickness, accompanied by a large increase in polar displacements (figure 3(b)). The role of electrostatic potential and surface adsorbates in the observed structural transition and in the stabilization of polar displacements (as well as the insulating character of these freestanding films) remain to be characterized, however, these advances hold promise for the study of structural reconstructions and the prevalence of ferroic order at the 2D limit in strongly correlated oxides.

4. Strain engineering of oxide membranes

The mechanical behavior of materials when approaching the 2D limit is often very different from that of a bulk crystal. For example, the breaking strength of graphite is limited by the presence of defects and grain boundaries, however, when monolayer graphene is isolated, one can reach the intrinsic strength of the material, which is one order of magnitude higher, and this has allowed researchers to tag graphene as 'the strongest material ever measured' [8]. In the case of complex oxides, single crystals and ceramics typically sustain very low strain levels before cracking (in the order of 0.1%), however, epitaxial thin films have been shown to withstand biaxial strains as high as 6% [128], although typical values for strain relaxation mechanisms via dislocation formation or cracking are around 1%–3%.

This strain tunability via epitaxial growth of TMO films has facilitated exploring the strong lattice coupling with charge, spin, and orbital degrees of freedom [39, 129] and helped identifying novel properties and phases by growing films on substrates with different lattice mismatch. Mixed-valence manganites have been extensively used as prototypical materials to explore epitaxial strain effects on electron correlations via lattice induced changes of orbital hybridization and corresponding modifications of charge localization and spin order [41, 130]. In FE films, on the other hand, mesoscopic domain ordering and polarization stability have been tuned via epitaxial strain to optimize dielectric, piezoelectric, or pyroelectric susceptibilities [131–133].

Using the epitaxial strain engineering approach, strain tunability typically requires finding a range of suitable substrates to induce different lattice deformations which involves the synthesis of a series of films which are often not fully comparable in terms of defects, morphologies, etc or the synthesis of films on piezoelectric single crystals that allow for electrical control of strains within a small range (<±1%).

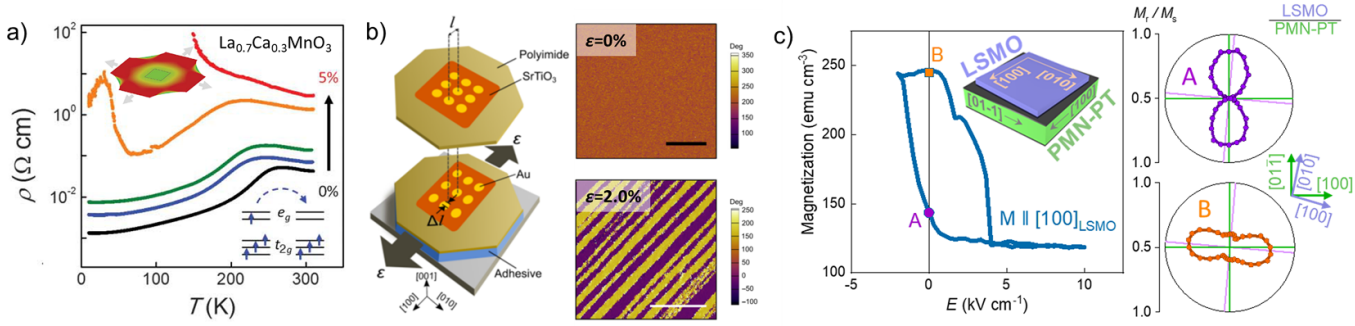

Figure 4. (a) Temperature-dependent resistivity of an 8 nm thick $La_{0.7}Ca_{0.3}MnO_3$ membrane as a function of biaxial strain applied to the polymer substrate (top left inset). Strain effectively suppresses electron hopping between manganese sites (bottom right inset). From [55]. Reprinted with permission from AAAS. (b) $SrTiO_3$ membrane uniaxially stretched on a polyimide sheet (left) leads to the emergence of ferroelectric domains at room temperature (right). Reproduced from [144]. CC BY 4.0. (c) Left: in-plane magnetization component of a $La_{0.7}Sr_{0.3}MnO_3$ (LSMO) membrane transferred to a $0.68Pb(Mg_{1/3}Nb_{2/3})O_3$–$0.32PbTiO_3$ (PMN-PT) substrate, versus electric field E applied to the substrate. Remanent states A (purple dot) and B (orange square) were obtained by electrically cycling the PMN-PT substrate in a minor loop. Right: polar plots of loop squareness M_r/M_s obtained for remanent states, indicating 90° rotation of magnetic easy axis. Reproduced from [134]. CC BY 4.0.

This is challenging, however, due to the (typically) large lattice mismatch between these piezoelectric substrates and the functional films of interest which leads to misfit dislocation formation and degradation of properties. Nevertheless, such a strain-actuation approach has been exploited for the dynamic manipulation of properties, such as electrical control of magnetization [135, 136], orbital order [137, 138], conductivity [139], photovoltaic effect [140], and FE polarization [141].

4.1. Tunable electron correlations via polymer stretching

Using the epitaxial lift-off strategy to release oxide membranes and transfer them to stretchable polymer substrates, researchers can now explore the whole elastic regime with a single membrane sample, without the need to synthesize/optimize growth of films on a range of substrates covering the accessible strain states. This was tested on a film of $La_{0.7}Ca_{0.3}MnO_3$ [55], a ferromagnetic metal in close proximity to insulating (anti-)ferromagnetic and charge-/orbital-ordered phases. The film, transferred to a polyimide sheet, could be stretched to staggering values of 8% strain for a uniaxial geometry and 5% strain for the biaxial configuration. The researchers then explored the magnetotransport properties of the membrane for different strain states induced by the uniform planar deformation of the substrate. Following this approach, a whole range of magnetic field, temperature, and strain could be explored in a single film, with resistivity modulations of more than two orders of magnitude (figure 4(a)) and large tunability of the phase-transition temperature between the ferromagnetic-metal (FMM) and paramagnetic-insulator phases, revealing wide control over bandwidth and exchange interactions. At the largest biaxial strain levels (not readily reached by epitaxial strain) a novel phase was found at low temperatures, where the FMM was turned into a charge-/orbital-ordered insulator, with a reversible transition back to the FMM phase under large magnetic fields, analogous to the phenomena found in narrow-bandwidth manganites [142]. This study thus demonstrated a powerful material testing platform for exploring complex phase diagrams and tuning electron correlations in oxides.

4.2. Control of polar order

The interest in this straining method later shifted to the control of polar order. On membranes of $SrTiO_3$, an incipient FE in which quantum fluctuations suppress ferroelectricity, it was found that a 2% strain applied uniaxially via polymer stretching induced significant signal in optical second harmonic generation (SHG) measurements, and a structure of in-plane polarized domains, indicative of a stabilized FE phase at room temperature [144] (figure 4(b)). For membranes of $PbTiO_3$ (a tetragonal FE at room temperature), a similar strategy was used to tune the domain orientation from predominantly out-of-plane to predominantly in-plane, as observed in x-ray diffraction measurements of the membranes under strain applied to the polymer substrate up to 6% [91]. For membranes of $BiFeO_3$, the same polarization rotation effect under uniaxial tensile strain was used to explain the large modulation in thermal resistance across the films, as measured via the thermoreflectance technique [143]. All these works represented an advance with respect to strain engineering in epitaxial films in that uniaxial strain (instead of biaxial) can be used, providing a maximum achievable strain that is 2–3 times larger than typical values in epitaxial films and the strain tunability is 1–2 orders of magnitude larger than that achievable via piezoelectric substrates [141], thus providing an excellent tool for manipulating structures and tuning electronic correlations to a large extent. One has to take into account, however, that these studies were made on ultrathin films (10 unit cells thick or less), whereas thicker films may be more prone to form dislocations and crack upon stretching due to the larger elastic energy put into the system. *In situ* electron microscope tensile testing experiments [145] would provide valuable insights into the microscopic mechanisms for strain accommodation in the

elastic regime, occurrence of plastic deformation and ultimate tensile strength in these membranes.

4.3. Dynamic strain control of functionalities

In contrast to epitaxial heterostructures [146], researchers have now shown that heterostructures made by transferring ferromagnetic manganite films to piezoelectric substrates of PMN-PT show no degradation of magnetic properties (i.e. bulk Curie temperature and magnetization) [134]. Moreover, despite the *a priori* weaker interface bonding, the magnetoelectric coupling coefficient for these heterostructures fabricated via epitaxial lift-off were similar to values reported on heteroepitaxial structures. Another interesting advantage of this approach is that the strain anisotropy—determined by the piezoelectric-substrate structure (phase/crystallographic orientation)—can be selected independently of the magnetic anisotropy (as determined by the magnetic film structure and morphology). This was exploited [134] to obtain two distinctive magnetic states at electrical remanence in (001)-oriented manganite films transferred to (110)-oriented PMN-PT substrates (figure 4(c)). Replacing the piezosubstrate with a piezoelectric film allows for low-voltage magnetic manipulation [147, 148], reverse operation (magnetic field induced voltage) [79] and potential CMOS and flexible integration of magnetoelectric memories [149]. These works may also help in devising smart strategies for electrical manipulation of magnetization exploiting interlayer misorientation [150, 151] or combining epitaxial magnetic metals with chemically incompatible epitaxial piezoelectric films [148] for highly efficient magnetoelectric spin-orbit logic memory devices.

Strain control can also be achieved via mechanical manipulation of the complex oxide membranes transferred onto flexible bendable platforms. Following this approach, researchers have demonstrated strain tuning of magnetic anisotropy in membranes of magnetostrictive $CoFe_2O_4$ on polyimide [109], modulation of the photovoltaic effect in membranes of FE $BiFeO_3$ on PDMS [152], or large conductivity changes in piezoresistive VO_2 on PET [107] upon bending of the polymer supports. These approaches for mechanical modulation of properties are highly interesting for applications in magnetic switches, self-powered energy harvesters, tactile sensors, and highly efficient health monitoring devices [107, 153–155].

Ultimately, careful choice of materials in which there exists a competition between (nearly) energetically degenerate phases that are easily destabilized by strain allows for large effects driven by small mechanical stress. Such is the case demonstrated on $Ba_{0.7}Sr_{0.3}TiO_3$ capacitors fabricated on PET, where small mechanical stress ($\pm 0.1\%$) applied by bending the polymer led to very large changes in the dielectric susceptibility (90%) [102]. Free energy calculations suggested that the transition between closely energetic domain configurations upon membrane straining account for the large dielectric tunability. This may motivate exploring these techniques in other highly susceptible materials, such as those close to morphotropic phase boundaries or in close proximity to phase transitions induced by strain or dimensionality [156, 157].

5. Superelastic deformations and flexoelectricity

Considering the brittle character of the often strongly ionic bonding in TMO structures, the stretchability of substrate-released membranes, as shown in the previous section, has surpassed researchers' expectations. This suggests fundamentally different elastic behavior at the nanoscale, and researchers are now focusing on exploring the elastic limits of these membranes and the microstructural arrangements allowing for their exceptional elasticity, as well as their influence on ferroic ordering.

5.1. Superelastic deformation in ferroelastic-FE membranes

Microstructural effects are especially relevant in ferroelastics, where large strains can be accommodated via twinning domains or via structural phase transformations, and the simultaneous occurrence of both can lead to superelastic deformations such as those found in shape-memory alloys, showing reversible strains as large as 13% [158]. Such structural rearrangements can also occur in FEs, where ferroelastic domains help minimize the total energy of the system, considering both electrostatic and elastic interactions. The degree of deformation achieved in FEs when applying a stress depends on the mobility of domains and their ability to accommodate internal stresses without producing mechanical failure or unstable polarization discontinuities. When domains become pinned, phase transformations may be triggered, enabling further elastic deformation [159], but for this to happen, closely energetic low-symmetry phases (morphotropic/thermotropic) [128, 160] must be accessible.

Freestanding FE-ferroelastic membranes were found to undergo large superelastic deformations during *in situ* bending tests, reaching 10% strain without fracture [56] (figure 5(a)). In $BaTiO_3$, cross-sectional TEM images of bent membranes revealed the presence of tetragonal *a* domains (in-plane extended) at the convex side and *c* domains (in-plane compressed) at the concave side, connected by continuous rotation of the dipoles [56, 161]. Phase-field simulations support these observations and suggest that vortex-like structures can be stabilized inside the bent membranes [162]. In contrast with these observations, similar bending experiments in $BaTiO_3$ single-crystal nano-pillars fabricated by FIB revealed the presence of more complex hierarchical domain structures and stress-induced bridging monoclinic phases, suggesting a different strain accommodation mechanism [159]. Phase coexistence was suggested as the main mechanism to accommodate the curvature in freestanding $BiFeO_3$ membranes, where—according to phase-field simulations—a rhombohedral phase appears in the compressive region and a tetragonal phase accommodates the strain in the tensile strained region, allowing researchers to reach the maximum bending strain of 5% observed in TEM [163, 164].

Spontaneous bending of the membranes can also be observed, if the mechanical boundary conditions at the top and bottom layers are different. Being free from substrate clamping, such mechanical boundary conditions can be affected by electrostatic considerations, such as depolarizing fields.

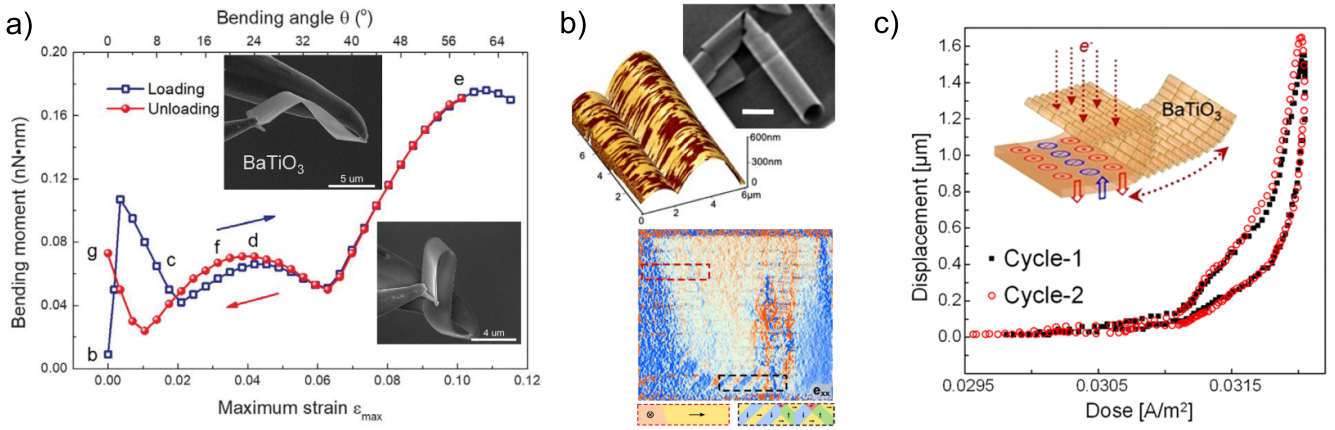

Figure 5. (a) Bending moment as a function of maximum strain (calculated from the bending angle) of a $BaTiO_3$ flake upon application and removal of a load. The insets show SEM images of the bent $BaTiO_3$ flake (20 μm by 4 μm by 120 nm. From [56]. Reprinted with permission from AAAS. (b) Left: lateral PFM phase image overlaid on the surface topography of freestanding $PbTiO_3/SrTiO_3$ superlattice tubes and an SEM image of the freestanding tubes (scale is 10 μm). Right: strain distribution map across the thickness of a tube, and sketches of the proposed domain structures in the highlighted regions. Reproduced from [165]. CC BY 4.0. (c) Reversible and repeatable piezoresponse of a folded $BaTiO_3$ freestanding membrane as illustrated by the change of the position of the fold as a function of the electron dosage in the TEM. Reprinted with permission from [166]. Copyright (2020) American Chemical Society.

This was observed in $PbTiO_3/SrTiO_3$ superlattices, where the strain-induced out-of-plane polarization in the epitaxial films is destabilized once the superlattice is released from the substrate, leading to in-plane polarization and flux-closure domains that eliminate the depolarizing field and causes large lattice mismatch with the bottom $SrRuO_3$ electrode and the curling of the membranes into microscopic rolls [165]. X-ray diffraction and cross-sectional TEM studies reveal the distribution of ferroelastic domains across the thickness of the superlattice rolls, as a mechanism for accommodating the curvature (figure 5(b)).

Direct electrical actuation in these membranes is challenging, however, surface-charge accumulation was proposed as a strategy for remote actuation in freestanding FE membranes [166]. It was observed that $BaTiO_3$ suspended flakes that were initially folded, unfold upon irradiation with the electron beam in TEM. The unfolding was found to progress linearly for low electron doses and abruptly for higher doses, and the initial folding state could be recovered reversibly, with a total displacement of the folding plane of >1 μm (figure 5(c)). This response was found to vanish at higher temperatures when the membrane is no longer FE, thus demonstrating that the giant piezoresponse is enabled by the charge manipulation of FE domains with nanoscale periodicity, easily switched by the induced charge.

These works demonstrate that membranes can sustain large bending deformations via multiple structural arrangements and are susceptible to display large electromechanical responses achieved via controllable electrostatic engineering of the curvature induced in the membranes.

5.2. *Strain-gradient engineering*

The demonstrated curvature control and superelastic deformation upon bending warrants further exploration of flexoelectric effects induced by the large strain gradients achievable in the membranes. The role of flexoelectricity (electric polarization induced by a strain gradient), while small in bulk crystals, becomes highly relevant at the nanoscale, strongly influencing electromechanical behavior in crystalline materials [167], which can be used to mechanically write [168] and read [169] bits of information, enhance the efficiency of processes such as photovoltaic effects [170], or develop nanoactuators exploiting the inverse effect (bending in response to electric field) [171]. Using advanced deposition methods, researchers can now synthesize epitaxial thin films with engineered strain gradients as large as $>10^5$ m^{-1} using compositional gradients, which has proven as an effective strategy to enhance susceptibilities (e.g. pyro-/piezoelectric) [172–174].

Freestanding membranes, on the other hand, are prone to wrinkle and buckle once released from the supporting substrate, leading to large local strain gradients in compositionally homogeneous films. One way to control the wrinkling/buckling parameters (i.e. the pattern periodicity, local curvature, amplitude, etc.), is to place the stiff membranes in contact with soft polymers. The elastic mismatch leads to a stress-driven instability, which induces wrinkled textures similar to those found in metal layers and 2D materials [175, 176]. $BaTiO_3$ membranes coupled to PDMS were shown to display a periodically alternating peak and valley morphology with curvatures in the order of a few μm^{-1}. Cross-sectional scanning TEM images revealed strain gradients in the film as large as 10^6 m^{-1}, that are accommodated through continuous dipole rotations across the thickness of the membranes, and that produce large local enhancement of polarization from flexoelectricity, as estimated from the barium-titanium displacements [161]. Such polymer-oxide bilayer systems may open the way for a novel 'texture engineering' approach where periodicity and strain gradients can be tuned by changing the thickness or stiffness ratio of the heterostructure, and different

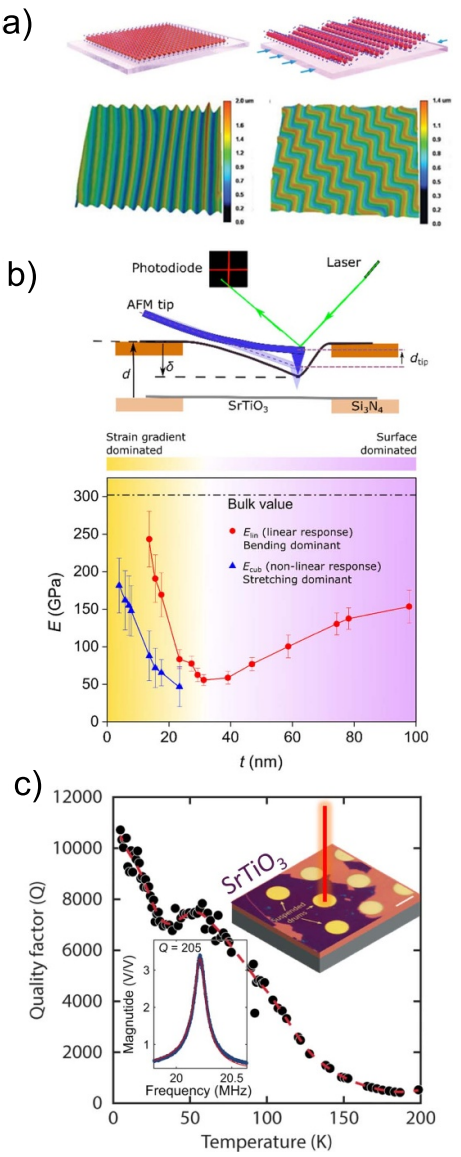

Figure 6. (a) Top: fabrication of oxide membranes with periodic wrinkle patterns induced by polymer pre-strain. Bottom: uniaxial (biaxial) pre-strain produces rectilinear (herringbone) wrinkle patterns ([110] John Wiley & Sons. [Copyright (2020) WILEY-VCH Verlag GmbH & Co. KGaA, Weinheim]). (b) Schematic of nanoindentation measurement on suspended $SrTiO_3$ drumheads and experimentally extracted Young's modulus associated to stretching and bending deformations, as a function of membrane thickness (reprinted with permission from [181]. Copyright (2021) American Chemical Society). (c) Quality factor corresponding to the mechanical resonance (shown in bottom inset) of a $SrTiO_3$ 4 μm diameter suspended drum (shown in top inset) as a function of temperature, showing anomalous behavior around 30 K, where small strontium displacements lead to a triclinic distortion and local emergence of polarity (reproduced from [182]. CC BY 4.0).

fold patterns (e.g. unidirectional or herringbone) (figure 6(a)) may be stabilized, with local functional responses modulated by the textured topography [177].

Nanoindentation procedures using a scanning force microscope also provide a convenient tool to reversibly bend freestanding membranes and simultaneously obtain mechanical information of the films [178, 179], which is not easily accessible in epitaxial systems. By measuring force-deflection curves in freestanding drumheads of $SrTiO_3$, it was found that these membranes can sustain more than one order of magnitude higher strain than in bulk, with a high endurance upon indentation cycling [180]. Such nanoindentation probing was also used to identify an elastic stiffening with a non-linear thickness dependence for membranes less than 30 nm in thickness, which was attributed to the electrostatic energy gain due to flexoelectrically induced polarization at reduced thicknesses (figure 6(b)) [181]. The large dielectric constant of $SrTiO_3$ makes it an ideal material candidate to observe flexoelectric-related effects, however, given that flexoelectricity is a universal material property, the phenomena identified in $SrTiO_3$ may play a role in other materials, especially in the 2D limit.

5.3. Nanomechanical resonators

Suspended membranes are also suitable for high-performance sensing devices, and multiphase materials with strong strain/strain gradient coupling are ideal to develop new concepts for multifunctional nanoelectromechanical systems. Using laser interferometry, it was demonstrated that $SrTiO_3$ and $SrRuO_3$ suspended drumheads display good performance as nanomechanical resonators with high quality factors at low temperatures [182]. The resonance frequency and attenuation factors were shown to be extremely sensitive to the internal structure of the membranes, and researchers were able to detect elastic anomalies associated to minute local structural distortions in $SrTiO_3$ at low temperatures, which are hardly detectable even in bulk crystals [183] (figure 6(c)), thus demonstrating a powerful tool to study phase transitions in ultrathin oxide films, analogous to more developed techniques in bulk materials [184]. This optomechanical approach also opens the door to combining nanomechanics with the plethora of electronic phases displayed by complex oxides.

6. Integrated devices

The successful demonstration of room-temperature coupling of single-crystal oxide nano-membranes with silicon [100] represents a milestone toward the fabrication of CMOS-compatible complex-oxide devices, using a method that is potentially scalable and cost-efficient [86, 87]. This technology also offers an opportunity to improve device functionalities previously hampered by elastic constraints, and to develop new device concepts based on combinations of materials and interfaces not achievable via conventional synthesis processes. The recent efforts summarized here represent a higher degree of materials control and a step forward in the implementation of oxides in next-generation devices.

6.1. CMOS and flexible integrated devices

Epitaxial lift-off techniques have been used to fabricate high-performance oxide devices on silicon and on polymer substrates. For example, an FE-FET device was demonstrated by using a PZT flake as the gate, showing good interface

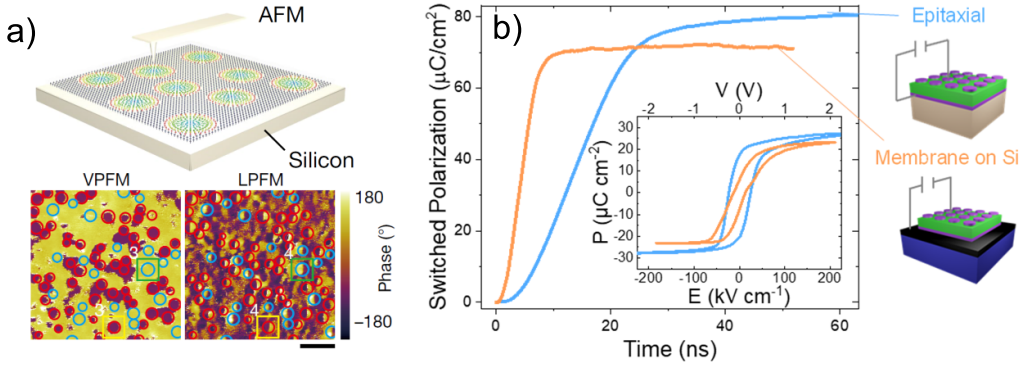

Figure 7. (a) $PbTiO_3/SrTiO_3$ membrane transferred to silicon displays a high density of center-divergent and center-convergent skyrmion-like nanodomains, respectively marked by red and blue circles in the vertical and lateral piezoresponse force microscopy phase images; scale bar is 100 nm. Reproduced from [187], with permission from Springer Nature. (b) Switched polarization after a switching voltage pulse of 1.9 V, for a 100 nm thick $BaTiO_3$ epitaxial capacitor (blue) and a 100 nm thick $BaTiO_3$ substrate-released capacitor on silicon (orange), both with 10 nm thick $SrRuO_3$ electrodes. The inset shows the ferroelectric polarization loops measured at 10 kHz. [102] John Wiley & Sons. [Copyright (2020) WILEY-VCH Verlag GmbH & Co. KGaA, Weinheim].

control over the SiO_2 channel current by switching the PZT polarization [100]. FE capacitors, at the core of nonvolatile random-access memories, can be epitaxially grown on oxide substrates and transferred to silicon, maintaining their high crystallinity and showing switching characteristics that are controllable via heterostructure design [102], or integrated on flexible polymer substrates [59], showing switching figures of merit (polarization, switching speed, fatigue) that overcome previous demonstrations on capacitors directly grown on ultrathin flexible silicon [185].

Likewise, polar topological structures found in epitaxial oxide heterostructures grown on oxide substrates [186], could also be transferred onto silicon. Bilayers of $PbTiO_3/SrTiO_3$ transferred to silicon were shown to display skyrmion-like polar domains with lateral sizes under 30 nm (figure 7(a)), which paves the way for the integration of topological structures with potentially high densities (e.g. more than 200 gigabits per square inch). Moreover, these polar nanostructures were found to show switchable, reversible, and non-volatile resistive behavior with two orders of magnitude change in the conductivity of the core of the nanodomains, between 'on' and 'off' states [187].

Researchers are also putting considerable effort into integrating high-κ perovskite oxides with 2D semiconductors. $SrTiO_3$ is an ideal material candidate to use as gate dielectric for field-effect transistors comprising high-mobility channels of van-der Waals semiconductors such as MoS_2. Epitaxial lift-off and transfer techniques have been demonstrated as suitable strategies to integrate such dissimilar materials into a high-performance transistor device, displaying on/off ratios as high as 10^8 [188, 189]. Expanding this strategy to FE oxides would provide opportunities, for example, to add non-volatile functionality or develop neuromorphic devices [190]. In this regard, binary oxides with fluorite structure are promising candidates for such applications: polycrystalline films of $Hf_{0.8}Zr_{0.2}O_2$ and ZrO_2 grown by atomic-layer deposition on silicon display FE behavior down to just a single unit cell [191, 192]; however, interface optimization, as well as integration of single crystal films may motivate researchers to expand the epitaxial lift-off techniques to fluorite based compounds.

FE tunnel junctions, which are memristive memories with voltage-controllable resistance and non-volatile operation, were also fabricated after transferring the epitaxial heterostructures to silicon [97] and to flexible polymers [60]. In both cases the reported devices showed comparable performance to epitaxially grown heterostructures, with large on-off ratios, good uniformity and repeatability, and multi-state operation (i.e. ideal characteristics for data storage applications and neuromorphic networks). Beyond FEs, the successful demonstration of high-quality membranes of high-mobility complex-oxide semiconductors [93], 2D electron gases [193], and high-temperature superconductors [96] offer alluring opportunities to integrate a wide variety of electronic functionalities with silicon-based architectures.

6.2. *Improved performance in transferred devices*

The mechanical clamping imposed by substrates in epitaxial heterostructures strongly limits the performance of (electro-/magneto-/photo-) strictive materials by inhibiting the elastic deformation in response to the applied field. The substrate clamping effect has been extensively studied in FE films [194, 195], as a limiting factor for their piezoresponse as well as for their poling ability, which plays a significant role in the thickness scalability of these materials and the energy required to activate polarization-switching processes. The role of the mechanical boundary conditions on the energetics and lattice dynamics of these systems was explored in detail in $BaTiO_3$ [102] and $BiFeO_3$ [104] capacitors fabricated on silicon after epitaxial lift-off and transfer. These works revealed how the removal of substrate bonding strongly alters the FE switching paths by facilitating structural distortions upon voltage application that were restricted by the substrate-imposed mechanical constraint. This, in turn, modifies the energy landscape during switching, significantly lowering the required voltage for polarization reversal and decreasing the switching times, thus potentially leading to faster and more power-efficient memory

devices (figure 7(b)). Other works [101, 196], however, have pointed at possible extrinsic mechanisms for domain-wall pinning and additional strain sources in PZT membranes, caused by rippled topographies and associated structural fluctuations, that may contribute to slower domain-wall velocities, but may help stabilizing topological-domain structures. Future work in these directions is expected to clarify the contribution of ferroelastic domains during the switching process and the local flexoelectric effects induced by spontaneous textures in the membranes.

7. Outlook—future possibilities

The rapid development of the processing, manipulation, structural and functional characterization, and device fabrication of complex-oxide membranes have led, in the last few years alone, to groundbreaking studies in the low-dimensional physics of these materials, with significant milestones (such as synthesis of 2D perovskite layers and superelastic behavior of freestanding membranes) that will strongly influence future work. Ultimately, the synergy between the communities of complex oxides and 2D materials is poised to bring together the wide range of physicochemical phenomena studied by the former and the expertise on materials manipulation near the 2D limit and van-der-Waals heterostructuring of the latter. Here, we outline some of the fields that may benefit from this synergy in the near future, leading to new synthetic materials, improved energy conversion strategies, innovative device concepts and deeper understanding of the mechanisms underlying the complex-oxide functionalities at the nanoscale.

7.1. Integration of multifunctional devices

Beyond electronic and logic applications, the multifunctional behavior of complex oxides comes in handy when envisioning novel devices such as electrooptical modulators using FE materials with large Pockels effect [197], pressure sensors based on manganite films with metal-to-insulator transitions [198], flexible biosensors employing piezoelectrics [153], or magnetic microwave devices using magnetoelectric heterostructures [199]. The fact that single-crystal oxide membranes transferred to flexible polymer substrates show magnetic and electrical properties comparable to their precursor epitaxial films, even under bending conditions [94, 200–202], opens a path toward implementing this fabrication technology in flexible, wearable electronics. In some cases, when epitaxial strain becomes detrimental to the oxides functionalities, the released membranes can even display improved performance, such as higher Curie temperature and magnetization in colossal magnetoresistance manganites [90, 134] or larger resistivity modulation in rutile oxides showing metal-to-insulator transitions [95, 108], which further encourages the development of multifunctional devices incorporating complex oxide membranes.

7.2. Lattice dynamics

The propagation of lattice vibrations in a solid depends on the elastic properties of the medium, as well as its boundary conditions. Measuring phonon dispersion relations would provide relevant insights into the lattice dynamics of freestanding-complex oxides, fundamental to understand their improved FE switching speeds [104] and explore photoinduced effects [203] or the role of microstructure and size scaling on functional properties [56, 58]. Time-resolved structural evolution upon application of an external field could be obtained using pump-probe techniques such as ultrafast electron diffraction which, although not suitable for epitaxial films on substrates, would be able to provide a complete picture of the structural dynamics of freestanding membranes in the femtosecond regime [204]. Such techniques could ultimately help understanding the intricate spatial and temporal correlations at the nanoscale in complex ferroic glass systems, where structural, chemical, charge, or spin disorder [205] can produce ultraresponsive materials, such as polar relaxors [206] and disclose the evolution of local order with temperature, applied field, or dimensionality [207, 208].

7.3. Thermal energy conversion

Ferroic oxides are among the materials currently being considered for solid-state refrigeration [209, 210] either via magnetocaloric [211], electrocaloric [212], or multicaloric effects [213] that originate from adiabatic temperature changes upon application of external fields (i.e. magnetic, electric, stress, or sequential application of these fields). Studying caloric effects in thin films is challenging, due to their low thermal mass, but worth pursuing, given the need for on-chip efficient refrigeration [214]. Giant caloric effects in thin films have been suggested by indirect calculations of temperature and entropy changes extracted from magnetization [215] and electrical polarization measurements [216], which in general disregard the temperature and field dependence of heat capacity. Films released from the substrate, which act as a thermal sink, provide an ideal platform to study caloric effects, by probing temperature changes directly via microfabricated electrothermal sensors [217] or infrared thermography [218, 219], or by accessing the specific heat involved in the process via fast scanning nanocalorimetry [220] or elasticity measurements [221]. Moreover, their superelastic behavior make them suitable for exploring elasto- or piezo-caloric effects (stress-induced effects), which are, as yet, poorly studied in oxides, but predicted to yield giant temperature changes, promoted by the large strain coupling with the order parameter around phase transition temperatures [222, 223]. The integration of oxide membranes on flexible substrates may inspire solutions to measure such mechanocaloric effects [224] or explore new effects such as flexocaloric [225].

Conversely, in the quest for high efficiency thermal sensors and imaging systems via thermal-to-electrical energy conversion [226, 227], epitaxial films have demonstrated high-performance pyroelectric-energy conversion [133, 228]. The study of freestanding films that avoid secondary pyroelectric effects arising from the thermal mismatch with the substrate [229] may promote new strategies for enhancing pyroelectric coefficients, as already observed in suspended polycrystalline films [230].

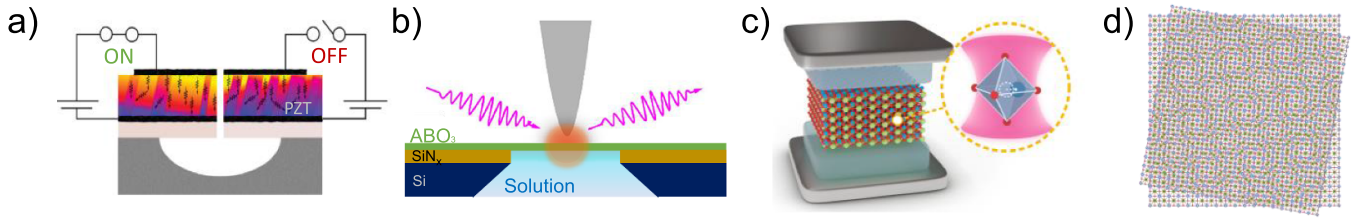

Figure 8. (a) Bistable thermal conductivity in suspended ferroelectric films, through voltage-reconfigurable domain-wall density. Reprinted with permission from [238]. Copyright (2018) American Chemical Society. (b) Schematic of a plasmonically enhanced infrared spectroscopy experiment at the liquid/complex-oxide interface. Reprinted with permission from [259]. Copyright (2020) American Chemical Society. (c) $SrTiO_3$ membrane integrated in an Fabry–Perot cavity and titanium-oxygen displacive motion induced by phonon coupling to the cavity photons. Reproduced from [243]. CC BY 4.0. (d) Stack of two rotated perovskite layers, forming a Moiré pattern.

7.4. Thermal transport

Phonon propagation is known to be affected by domain microstructures in ferroic oxides, where domain walls may act as reconfigurable phonon scatterers [231], thus providing a strategy for regulation of heat transport at the nanoscale (figure 8(a)) [232], and, ultimately, use phonons as fundamental computing units in thermal logic devices [233]. So far, the proven efficiency of this strategy has been poor, with only small changes of thermal conductivity reported upon application of electric field in FE thin films [234, 235]; however, smart domain engineering [236, 237] and substrate declamping [238] may hold the key for optimizing thermal regulation performance of ferroic oxides. The fabrication of freestanding nanomembranes via epitaxial lift-off and the well-developed techniques for thermal characterization of nanostructures [239] provide the two main ingredients necessary for success in this direction.

7.5. Light-matter interactions

Nonlinear and transient optical properties of TMO may become more pronounced and tuneable in membranes which are free of substrate clamping, heat, and optical absorption. For example, one can think of an optically switchable SHG, where the excitation pulse energy is tuned to drive the freestanding membrane through an FE-to-paraelectric phase transition. On the other hand, efficient absorption in the freestanding membranes could stabilize the optically induced transient phases, such as metastable ferroelectricity in paraelectric $SrTiO_3$ [240] or superconductivity in cuprates [241]. These phases are induced by targeting a specific mid-infrared phonon in TMO [242], yet substrate clamping can increase the phonon decay rates making the suspended samples preferrable to prolong the phase lifetimes. Moreover, the symmetric geometry of the freestanding TMO membranes would allow for the creation of nanocavities for the material's phase control via interaction with the photon vacuum fields that would not require direct optical pumping (figure 8(b)) [243].

TMO membrane approaches would facilitate the integration of switchable $LiNbO_3$ waveguides [244] with technologically incompatible CMOS or flexible substrates with a range of quantum technology and telecom applications [245]. Another way to harness the quantum potential of TMO materials is through the creation and manipulation of coherent excitations such as phonon-polaritons (PhPs). The high intensity of the light–matter interaction is crucial for the stability of these quasiparticles and can be attained by confining photonic modes in a small material volume, making thin films good candidates for PhP observation. While the high quality factor PhPs have been observed in intrinsically layered MoO_3 flakes [246], highly confined PhPs are also predicted in the monolayer films of non-layered TMOs [247]. Surface PhPs have been recently observed in $SrTiO_3$ [248] in a wide range of frequencies from THz to mid-infrared. Moreover, the artificial TMO superlattices exhibit hyperbolic properties [249] which can serve as a precursor for the confined PhPs.

In general, the possibility of substrate decoupling, and transfer onto an arbitrary surface or even full suspension paves the way to enhanced light-matter interactions in membrane TMO leading to the engineering of new material phases as well as simply incorporating the existing functional phases into the CMOS technology and metamaterials.

7.6. Electrochemistry

TMO perovskites are well known catalyzers of different relevant chemical and electrochemical reactions [36]. The oxygen-reduction activity has been the main focus of study on complex oxides and is easily tailorable via chemical doping [250]. Epitaxial thin film synthesis has enabled accurate control over surface structures, atomic termination, and crystal facet orientation [35, 129, 251, 252], thus offering new routes to explore and tune surface reactivity and gas-exchange kinetics, crucial to identify optimal parameters for operation on solid-oxide fuel cells and electrolyzers. Reactions involving water splitting have also been identified on the surface of FE oxides [253–255], which hints at their application in hydrogen production. Moreover, the observed coupling of internal polarization to the surface chemical reactivity opens the way to explore pyrocatalytic or photocatalytic processes. The new tools described in this review to produce freestanding complex-oxide membranes would enable: (a) Increasing the surface-to-volume ratio by (e.g. by using rolled-up nanomembrane tubes [56, 95], (b) Accessing extreme-strain states where theory predicts increasing favorability of surface oxygen dissociation [256] but are not accessible in epitaxial heterostructures, (c) Actively tuning the catalytic activity via mechanical actuation [257], (d) Using mechanical detection

methods to identify strains associated with catalytic processes [258], (e) Fabricating electrocatalytic cells to characterize the atomic and electronic structure of metal-oxide compounds interfaced with gases and liquids, using ambient pressure conditions (figure 8(c)) [259, 260].

7.7. Moiretronics

The overlap of materials with dissimilar crystal periodicities or of the same periodicity but with an arbitrary twist angle gives rise to moiré superlattices. Moiré engineering has been extremely fruitful in the field of van der Waals 2D materials where it allowed one to induce flat electron bands in 'magic' angle twisted bilayer graphene leading to superconductivity and correlated insulator states [11, 12, 261]. Moiré superstructures have been recently observed in epitaxially grown systems, created via combination of substrate miscut steps and twin domains in the film [262], or via structural relaxation of a film on a closely lattice-matched substrate [263]. However, the fabrication of heterostructures via transfer of TMO membranes will permit a wider range of lattice combinations and include rotations (figure 8(d)). More efforts need to be put into eliminating interfacial residual layers found at oxide interfaces created by these transfer methods [79, 134]: e.g. post-annealing methods may help rendering cleaner interfaces or even form chemical bonds between the adjoining materials, as hinted at interfaces between TMO membranes and SiO_2 [260]. Nevertheless, such moiré heterostructures in TMOs are a promising path to exciting new discoveries, such as novel magnetization switching paths under electric field in twisted magnetoelectric heterostructures [151], or topological protection in high-T_C superconductors [264].

Data availability statement

No new data were created or analyzed in this study.

Acknowledgments

D P acknowledges the support of the European Union's Horizon 2020 research and innovation programmes under Grant agreements No. 797123 (Marie Skłodowska-Curie FERROENERGY) and No. 964931 (TSAR), funding from 'la Caixa' Foundation fellowship (ID 100010434), the Spanish Ministry of Industry, Economy and Competitiveness (MINECO) through Grant No. PID2019-108573GB-C21, the CERCA programme (Generalitat de Catalunya) and the 'Severo Ochoa' programme for Centers of Excellence in R&D of MINECO (Grant No. SEV-2017-0706). E K acknowledges funding from BIST-FBA fellowship. D P and E K acknowledge support of BIST Ignite Grant (TeraFox). The work at Berkeley acknowledges the support of the Army Research Office under Grants W911NF-21-1-0118, W911NF-21-1-0126, and under the ETHOS MURI via cooperative agreement W911NF-21-2-0162, the Army Research Laboratory via the Collaborative for Hierarchical Agile and Responsive Materials (CHARM) under cooperative agreement W911-NF-19-2-0119, the U.S. Department of Energy, Office of Science, Office of Basic Energy Sciences, Materials Sciences and Engineering Division under Contract No. DE-AC02-05-CH11231 (Materials Project program KC23MP), the U.S. Department of Energy, Office of Science for support of microelectronics research under Contract No. DE-AC02-05-CH11231, the U.S. Department of Energy, Office of Science, Office of Basic Energy Sciences, under Award Number DE-SC-0012375, and the National Science Foundation under Grants DMR-1708615 and DMR-2102895. Matteo Ceccanti is acknowledged for assistance with figure illustrations.

References

[1] Geim A K *et al* 2007 *Nat. Mater.* **6** 183–91
[2] Novoselov K S, Mishchenko A, Carvalho A and Castro Neto A H 2016 *Science* **353** aac9439
[3] Yankowitz M, Xue J, Cormode D, Sanchez-Yamagishi J D, Watanabe K, Taniguchi T, Jarillo-Herrero P, Jacquod P and LeRoy B J 2012 *Nat. Phys.* **8** 382–6
[4] Straus D B and Kagan C R 2022 *Annu. Rev. Phys. Chem.* **73** 403–28
[5] Geim A K and Grigorieva I V 2013 *Nature* **499** 419–25
[6] Li L J, O'Farrell E C T, Loh K P, Eda G, Özyilmaz B and Castro Neto A H 2016 *Nature* **529** 185–9
[7] Mak K F, Lee C, Hone J, Shan J and Heinz T F 2010 *Phys. Rev. Lett.* **105** 136805
[8] Lee C, Wei X, Kysar J W and Hone J 2008 *Science* **321** 385–8
[9] Ren Y, Qiao Z and Niu Q 2016 *Rep. Prog. Phys.* **79** 066501
[10] Roldán R, Castellanos-Gomez A, Cappelluti E and Guinea F 2015 *J. Phys.: Condens. Matter* **27** 313201
[11] Cao Y *et al* 2018 *Nature* **556** 80–84
[12] Cao Y, Fatemi V, Fang S, Watanabe K, Taniguchi T, Kaxiras E and Jarillo-Herrero P 2018 *Nature* **556** 43–50
[13] Cao Y, Park J M, Watanabe K, Taniguchi T and Jarillo-Herrero P 2021 *Nature* **595** 526–31
[14] Woods C R, Ares P, Nevison-Andrews H, Holwill M J, Fabregas R, Guinea F, Geim A K, Novoselov K S, Walet N R and Fumagalli L 2021 *Nat. Commun.* **12** 347
[15] Weston A *et al* 2020 *Nat. Nanotechnol.* **15** 592–7
[16] Catalan G 2008 *Phase Trans.* **81** 729–49
[17] Catalan G and Scott J F 2009 *Adv. Mater.* **21** 2463–85
[18] Gao R *et al* 2020 *Adv. Mater.* **32** 1905178
[19] Salamon M and Jaime M 2001 *Rev. Mod. Phys.* **73** 583–628
[20] Reyren N *et al* 2007 *Science* **317** 1196–9
[21] Sun C, Alonso J A and Bian J 2021 *Adv. Energy Mater.* **11** 2000459
[22] Goodenough J B 2001 *Localized to Itinerant Electronic Transition in Perovskite Oxides* vol 98 (Berlin: Springer)
[23] Ngai J H, Walker F J and Ahn C H 2014 *Annu. Rev. Mater. Res.* **44** 1–17
[24] Imada M *et al* 1998 *Rev. Mod. Phys.* **70** 1039–263
[25] Christen H M and Eres G 2008 *J. Phys.: Condens. Matter* **20** 264005
[26] MacManus-Driscoll J L, Wells M P, Yun C, Lee J-W, Eom C-B and Schlom D G 2020 *APL Mater.* **8** 040904
[27] Brahlek M, Gupta A S, Lapano J, Roth J, Zhang H-T, Zhang L, Haislmaier R and Engel-Herbert R 2018 *Adv. Funct. Mater.* **28** 1702772
[28] Schlom D G, Chen L-Q, Fennie C J, Gopalan V, Muller D A, Pan X, Ramesh R and Uecker R 2014 *MRS Bull.* **39** 118–30
[29] Rijnders G and Blank D H A 2005 *Nature* **433** 369–70
[30] Mannhart J and Schlom D G 2010 *Science* **327** 1607–11

[31] Hwang H Y, Iwasa Y, Kawasaki M, Keimer B, Nagaosa N and Tokura Y 2012 *Nat. Mater.* **11** 103–13
[32] Stemmer S and Millis A J 2013 *MRS Bull.* **38** 1032–9
[33] Boris A V *et al* 2011 *Science* **332** 937–40
[34] Pesquera D, Herranz G, Barla A, Pellegrin E, Bondino F, Magnano E, Sánchez F and Fontcuberta J 2012 *Nat. Commun.* **3** 1189
[35] Gao R *et al* 2021 *Adv. Mater.* **33** 2100977
[36] Shao-Horn Y *et al* 2017 *Science* **358** 751–6
[37] Vailionis A, Boschker H, Siemons W, Houwman E P, Blank D H A, Rijnders G and Koster G 2011 *Phys. Rev.* B **83** 064101
[38] Weber M C *et al* 2016 *Phys. Rev.* B **94** 014118
[39] Tokura Y and Nagaosa N 2000 *Science* **288** 462–8
[40] Baena A, Brey L and Calderón M J 2011 *Phys. Rev.* B **83** 064424
[41] Pesquera D *et al* 2016 *Phys. Rev. Appl.* **6** 034004
[42] Damodaran A R *et al* 2017 *Adv. Mater.* **29** 1702069
[43] Nelson C T *et al* 2011 *Science* **334** 968–71
[44] Zheng H *et al* 2004 *Science* **303** 661–3
[45] Vila-Fungueiriño J M *et al* 2015 *Front. Phys.* **3** 38
[46] Kumah D P, Ngai J H and Kornblum L 2020 *Adv. Funct. Mater.* **30** 1901597
[47] Scigaj M, Dix N, Fina I, Bachelet R, Warot-Fonrose B, Fontcuberta J and Sánchez F 2013 *Appl. Phys. Lett.* **102** 112905
[48] Reiner J W *et al* 2010 Advanced Materials **22** 2919–38
[49] Bitla Y and Chu Y-H 2017 *FlatChem* **3** 26–42
[50] Chu Y-H 2017 *npj Quantum Mater.* **2** 67
[51] Liu Y, Huang Y and Duan X 2019 *Nature* **567** 323–33
[52] Loehlin D W and Werren J H 2012 *Science* **335** 943–7
[53] Radisavljevic B, Radenovic A, Brivio J, Giacometti V and Kis A 2011 *Nat. Nanotechnol.* **6** 147–50
[54] Chang H-Y, Yang S, Lee J, Tao L, Hwang W-S, Jena D, Lu N and Akinwande D 2013 *ACS Nano* **7** 5446–52
[55] Hong S S *et al* 2020 *Science* **368** 71–76
[56] Dong G *et al* 2019 *Science* **366** 475–9
[57] Hong S S, Yu J H, Lu D, Marshall A F, Hikita Y, Cui Y and Hwang H Y 2017 *Sci. Adv.* **3** eaao5173
[58] Ji D *et al* 2019 *Nature* **570** 87–90
[59] Bakaul S R, Serrao C R, Lee O, Lu Z, Yadav A, Carraro C, Maboudian R, Ramesh R and Salahuddin S 2017 *Adv. Mater.* **29** 1605699
[60] Luo Z-D, Peters J J P, Sanchez A M and Alexe M 2019 *ACS Appl. Mater. Interfaces* **11** 23313–9
[61] Damodaran A R, Agar J C, Pandya S, Chen Z, Dedon L, Xu R, Apgar B, Saremi S and Martin L W 2016 *J. Phys.: Condens. Matter* **28** 263001
[62] Spreitzer M *et al* 2021 *APL Mater.* **9** 040701
[63] Gao W *et al* 2020 *J. Mater.* **6** 1–16
[64] Nicolosi V, Chhowalla M, Kanatzidis M G, Strano M S and Coleman J N 2013 *Science* **340** 72–75
[65] Osada M and Sasaki T 2009 *J. Mater. Chem.* **19** 2503
[66] Wang L and Sasaki T 2014 *Chem. Rev.* **114** 9455–86
[67] Ida S, Ogata C, Unal U, Izawa K, Inoue T, Altuntasoglu O and Matsumoto Y 2007 *J. Am. Chem. Soc.* **129** 8956–7
[68] Li D, Zhao H, Li L, Mao B, Chen M, Shen H, Shi W, Jiang D and Lei Y 2018 *Adv. Funct. Mater.* **28** 1806284
[69] Li S, Zhang Y, Yang W, Liu H and Fang X 2020 *Adv. Mater.* **32** 1905443
[70] Moore R G, Zhang J, Nascimento V B, Jin R, Guo J, Wang G T, Fang Z, Mandrus D and Plummer E W 2007 *Science* **318** 615–9
[71] Lee J *et al* 2006 *Nature* **442** 546–50
[72] Novoselov K S, Jiang D, Schedin F, Booth T J, Khotkevich V V, Morozov S V and Geim A K 2005 *Proc. Natl Acad. Sci. USA* **102** 10451–3
[73] Huang Y, Sutter E, Shi N N, Zheng J, Yang T, Englund D, Gao H-J and Sutter P 2015 *ACS Nano* **9** 10612–20
[74] Huang Y *et al* 2020 *Nat. Commun.* **11** 2453
[75] Wang X, You L X, Xie X M, Lin C T and Jiang M H 2012 *J. Raman Spectrosc.* **43** 949–53
[76] Sandilands L J, Shen J X, Chugunov G M, Zhao S Y F, Ono S, Ando Y and Burch K S 2010 *Phys. Rev.* B **82** 064503
[77] Zhang B Y, Xu K, Yao Q, Jannat A, Ren G, Field M R, Wen X, Zhou C, Zavabeti A and Ou J Z 2021 *Nat. Mater.* **20** 1073–8
[78] Bedell S W, Fogel K, Lauro P, Shahrjerdi D, Ott J A and Sadana D 2013 *J. Phys. D: Appl. Phys.* **46** 152002
[79] Kum H S *et al* 2020 *Nature* **578** 75–81
[80] Sambri A *et al* 2020 *Adv. Funct. Mater.* **30** 1909964
[81] Dahm R T, Erlandsen R, Trier F, Sambri A, Gennaro E D, Guarino A, Stampfer L, Christensen D V, Granozio F M and Jespersen T S 2021 *ACS Appl. Mater. Interfaces* **13** 12341–6
[82] Kum H, Lee D, Kong W, Kim H, Park Y, Kim Y, Baek Y, Bae S-H, Lee K and Kim J 2019 *Nat. Electron.* **2** 439–50
[83] Kong W *et al* 2018 *Nat. Mater.* **17** 999–1004
[84] Kim J, Bayram C, Park H, Cheng C-W, Dimitrakopoulos C, Ott J A, Reuter K B, Bedell S W and Sadana D K 2014 *Nat. Commun.* **5** 4836
[85] Yablonovitch E, Gmitter T, Harbison J P and Bhat R 1987 *Appl. Phys. Lett.* **51** 2222–4
[86] Sickmiller M *et al IEEE/LEOS 1995 Digest of the LEOS Summer Topical Meetings. Flat Panel Display Technology* (IEEE) pp 5–6
[87] Lush G B *et al* 1993 *Conf. Record 23rd IEEE Photovoltaic Specialists Conf.—1993 (Cat. No. 93CH3283-9)* (IEEE) pp 1343–6
[88] Gan Q, Rao R A, Eom C B, Garrett J L and Lee M 1998 *Appl. Phys. Lett.* **72** 978–80
[89] Paskiewicz D M, Sichel-Tissot R, Karapetrova E, Stan L and Fong D D 2016 *Nano Lett.* **16** 534–42
[90] Lu D, Baek D J, Hong S S, Kourkoutis L F, Hikita Y and Hwang H 2016 *Nat. Mater.* **15** 1255–60
[91] Han L, Fang Y, Zhao Y, Zang Y, Gu Z, Nie Y and Pan X 2020 *Adv. Mater. Interfaces* **7** 1901604
[92] Lu Z, Liu J, Feng J, Zheng X, Yang L-H, Ge C, Jin K-J, Wang Z and Li R-W 2020 *APL Mater.* **8** 051105
[93] Singh P, Swartz A, Lu D, Hong S S, Lee K, Marshall A F, Nishio K, Hikita Y and Hwang H Y 2019 *ACS Appl. Electron. Mater.* **1** 1269–74
[94] Jin C *et al* 2021 *Adv. Sci.* **8** 2102178
[95] Han K *et al* 2021 *ACS Appl. Mater. Interfaces* **13** 16688–93
[96] Chen Z, Wang B Y, Goodge B H, Lu D, Hong S S, Li D, Kourkoutis L F, Hikita Y and Hwang H Y 2019 *Phys. Rev. Mater.* **3** 060801
[97] Lu D, Crossley S, Xu R, Hikita Y and Hwang H Y 2019 *Nano Lett.* **19** 3999–4003
[98] Salles P, Caño I, Guzman R, Dore C, Mihi A, Zhou W and Coll M 2021 *Adv. Mater. Interfaces* **8** 2001643
[99] Li D, Adamo C, Wang B Y, Yoon H, Chen Z, Hong S S, Lu D, Cui Y, Hikita Y and Hwang H Y 2021 *Nano Lett.* **21** 4454–60
[100] Bakaul S R *et al* 2016 *Nat. Commun.* **7** 10547
[101] Bakaul S R *et al* 2020 *Adv. Mater.* **32** 1907036
[102] Pesquera D *et al* 2020 *Adv. Mater.* **32** 2003780
[103] Adamo C *et al* 2009 *Appl. Phys. Lett.* **95** 112504
[104] Shi Q *et al* 2022 *Nat. Commun.* **13** 1110
[105] Takahashi R and Lippmaa M 2020 *ACS Appl. Mater. Interfaces* **12** 25042–9
[106] Lee D K, Kim S, Oh S, Choi J-Y, Lee J-L and Yu H K 2017 *Sci. Rep.* **7** 8716
[107] Li X, Yin Z, Zhang X, Wang Y, Wang D, Gao M, Meng J, Wu J and You J 2019 *Adv. Mater. Technol.* **4** 1800695
[108] Lee D K, Park Y, Sim H, Park J, Kim Y, Kim G-Y, Eom C-B, Choi S-Y and Son J 2021 *Nat. Commun.* **12** 5019

[109] Zhang Y *et al* 2017 *ACS Nano* **11** 8002–9
[110] Dong G *et al* 2020 *Adv. Mater.* **32** 2004477
[111] Zhang B *et al* 2021 *Nano-Micro Lett.* **13** 39
[112] Meitl M A *et al* 2006 Nature Materials **5** 33–38
[113] Pizzocchero F, Gammelgaard L, Jessen B S, Caridad J M, Wang L, Hone J, Bøggild P and Booth T J 2016 *Nat. Commun.* **7** 11894
[114] Son S *et al* 2020 *2D Mater.* **7** 041005
[115] Zhao Q, Wang T, Ryu Y K, Frisenda R and Castellanos-Gomez A 2020 *J. Phys. Mater.* **3** 016001
[116] Martanov S G, Zhurbina N K, Pugachev M V, Duleba A I, Akmaev M A, Belykh V V and Kuntsevich A Y 2020 *Nanomaterials* **10** 2305
[117] Purdie D G, Pugno N M, Taniguchi T, Watanabe K, Ferrari A C and Lombardo A 2018 *Nat. Commun.* **9** 5387
[118] Suntivich J, Gasteiger H A, Yabuuchi N, Nakanishi H, Goodenough J B and Shao-Horn Y 2011 *Nat. Chem.* **3** 546–50
[119] Jalili H, Han J W, Kuru Y, Cai Z and Yildiz B 2011 *J. Phys. Chem. Lett.* **2** 801–7
[120] Santander-Syro A F *et al* 2011 *Nature* **469** 189–93
[121] Carlsson J M 2007 *Nat. Mater.* **6** 801–2
[122] Fasolino A, Los J H and Katsnelson M I 2007 *Nat. Mater.* **6** 858–61
[123] Ghosez P and Rabe K M 2000 *Appl. Phys. Lett.* **76** 2767–9
[124] Junquera J and Ghosez P 2003 *Nature* **422** 506–9
[125] Kim Y S *et al* 2005 *Appl. Phys. Lett.* **86** 102907
[126] Zhang Y, Li G-P, Shimada T, Wang J and Kitamura T 2014 *Phys. Rev.* B **90** 184107
[127] Wang H *et al* 2018 *Nat. Commun.* **9** 3319
[128] Zeches R J *et al* 2009 *Science* **326** 977–80
[129] Hwang J *et al* 2019 *Mater. Today* **31** 100–18
[130] Konishi Y, Fang Z, Izumi M, Manako T, Kasai M, Kuwahara H, Kawasaki M, Terakura K and Tokura Y 1999 *J. Phys. Soc. Japan* **68** 3790–3
[131] Kim J *et al* 2019 *Adv. Mater.* **31** 1901060
[132] Agar J C *et al* 2014 *Adv. Mater. Interfaces* **1** 1400098
[133] Pandya S, Wilbur J, Kim J, Gao R, Dasgupta A, Dames C and Martin L W 2018 *Nat. Mater.* **17** 432–8
[134] Pesquera D *et al* 2020 *Nat. Commun.* **11** 3190
[135] Eerenstein W, Wiora M, Prieto J L, Scott J F and Mathur N D 2007 *Nat. Mater.* **6** 348–51
[136] Thiele C, Dörr K, Fähler S, Schultz L, Meyer D C, Levin A A and Paufler P 2005 *Appl. Phys. Lett.* **87** 262502
[137] Aetukuri N B *et al* 2013 *Nat. Phys.* **9** 661–6
[138] Vasili H B, Pesquera D, Valvidares M, Gargiani P, Pellegrin E, Bondino F, Magnano E, Barla A and Fontcuberta J 2020 *Phys. Rev. Mater.* **4** 044404
[139] Heo S, Oh C, Eom M J, Kim J S, Ryu J, Son J and Jang H M 2016 *Sci. Rep.* **6** 22228
[140] Zhang W *et al* 2015 *Nano Energy* **18** 315–24
[141] Guo E, Roth R, Herklotz A, Hesse D and Dörr K 2015 *Adv. Mater.* **27** 1615–8
[142] Tomioka Y, Asamitsu A, Kuwahara H, Moritomo Y and Tokura Y 1996 *Phys. Rev.* B **53** R1689–92
[143] Zang Y *et al* 2022 *Adv. Mater.* **34** 2105778
[144] Xu R *et al* 2020 *Nat. Commun.* **11** 3141
[145] Cao K *et al* 2020 *Nat. Commun.* **11** 1–7
[146] Dörr K, Thiele C, Kim J-W, Bilani O, Nenkov K and Schultz L 2007 *Phil. Mag. Lett.* **87** 269–78
[147] Lindemann S *et al* 2021 *Sci. Adv.* **7** eabh2294
[148] Zhao W *et al* 2021 *Adv. Funct. Mater.* **31** 2105068
[149] Zhao Y *et al* 2021 *Adv. Funct. Mater.* **31** 2009376
[150] Peng R-C, Hu J-M, Momeni K, Wang J-J, Chen L-Q and Nan C-W 2016 *Sci. Rep.* **6** 27561
[151] Wang J, Yang T-N, Wang B, Rzchowski M S, Eom C-B and Chen L-Q 2021 *Adv. Theory Simul.* **4** 2000215
[152] Guo R *et al* 2020 *Nat. Commun.* **11** 2571
[153] Hwang G-T, Byun M, Jeong C K and Lee K J 2015 *Adv. Healthcare Mater.* **4** 646–58
[154] Qi Y, Kim J, Nguyen T D, Lisko B, Purohit P K and McAlpine M C 2011 *Nano Lett.* **11** 1331–6
[155] Dagdeviren C *et al* 2014 *Nat. Commun.* **5** 4496
[156] Roy Chaudhuri A, Arredondo M, Hähnel A, Morelli A, Becker M, Alexe M and Vrejoiu I 2011 *Phys. Rev.* B **84** 054112
[157] Boldyreva K *et al* 2007 *Appl. Phys. Lett.* **91** 2005–8
[158] Tanaka Y, Himuro Y, Kainuma R, Sutou Y, Omori T and Ishida K 2010 *Science* **327** 1488–90
[159] Deng Y *et al* 2019 *Acta Mater.* **181** 501–9
[160] Lummen T T A *et al* 2014 *Nat. Commun.* **5** 3172
[161] Dong G *et al* 2020 *Adv. Mater.* **32** 2004477
[162] Guo C, Dong G, Zhou Z, Liu M, Huang H, Hong J and Wang X 2020 *Appl. Phys. Lett.* **116** 152903
[163] Peng B *et al* 2020 *Sci. Adv.* **6** eaba5847
[164] Peng R-C, Cheng X, Peng B, Zhou Z, Chen L-Q and Liu M 2021 *Acta Mater.* **208** 116689
[165] Li Y *et al* 2022 *Adv. Mater.* **34** 2106826
[166] Elangovan H, Barzilay M, Seremi S, Cohen N, Jiang Y, Martin L W and Ivry Y 2020 *ACS Nano* **14** 5053–60
[167] Catalan G, Lubk A, Vlooswijk A H G, Snoeck E, Magen C, Janssens A, Rispens G, Rijnders G, Blank D H A and Noheda B 2011 *Nat. Mater.* **10** 963–7
[168] Lu H, Bark C-W, Esque de Los Ojos D, Alcala J, Eom C B, Catalan G and Gruverman A 2012 *Science* **336** 59–61
[169] Cordero-Edwards K, Domingo N, Abdollahi A, Sort J and Catalan G 2017 *Adv. Mater.* **29** 1702210
[170] Yang M-M, Kim D J and Alexe M 2018 *Science* **360** 904–7
[171] Bhaskar U K, Banerjee N, Abdollahi A, Wang Z, Schlom D G, Rijnders G and Catalan G 2016 *Nat. Nanotechnol.* **11** 263–6
[172] Mangalam R V K, Agar J C, Damodaran A R, Karthik J and Martin L W 2013 *ACS Appl. Mater. Interfaces* **5** 13235–41
[173] Agar J C *et al* 2016 *Nat. Mater.* **15** 549–56
[174] Damodaran A R *et al* 2017 *Nat. Commun.* **8** 14961
[175] Bowden N, Brittain S, Evans A G, Hutchinson J W and Whitesides G M 1998 *Nature* **393** 146–9
[176] Chen W, Gui X, Yang L, Zhu H and Tang Z 2019 *Nanoscale Horiz.* **4** 291–320
[177] Zhou Y *et al* 2022 *Nano Lett.* **22** 2859–66
[178] López-Polín G, Gómez-Navarro C, Parente V, Guinea F, Katsnelson M, Pérez-Murano F and Gómez-Herrero J 2015 *Nat. Phys.* **11** 26–31
[179] Khestanova E, Guinea F, Fumagalli L, Geim A K and Grigorieva I V 2016 *Nat. Commun.* **7** 12587
[180] Harbola V, Xu R, Crossley S, Singh P and Hwang H Y 2021 *Appl. Phys. Lett.* **119** 053102
[181] Harbola V, Crossley S, Hong S S, Lu D, Birkhölzer Y A, Hikita Y and Hwang H Y 2021 *Nano Lett.* **21** 2470–5
[182] Davidovikj D *et al* 2020 *Commun. Phys.* **3** 163
[183] Scott J F, Salje E K H and Carpenter M A 2012 *Phys. Rev. Lett.* **109** 187601
[184] Carpenter M A 2015 *J. Phys.: Condens. Matter* **27** 263201
[185] Ghoneim M T, Zidan M A, Alnassar M Y, Hanna A N, Kosel J, Salama K N and Hussain M M 2015 *Adv. Electron. Mater.* **1** 1500045
[186] Lu X 2019 *et al Nat. Commun.* **10** 3951
[187] Han L *et al* 2022 *Nature* **603** 63–67
[188] Yang A J *et al* 2022 *Nat. Electron.* **5** 233–40
[189] Huang J-K *et al* 2022 *Nature* **605** 262–7
[190] Luo Z, Yang M-M, Liu Y and Alexe M 2021 *Adv. Mater.* **33** 2005620
[191] Cheema S S *et al* 2020 *Nature* **580** 478–82
[192] Cheema S S *et al* 2022 *Science* **376** 648–52
[193] Eom K, Yu M, Seo J, Yang D, Lee H, Lee J-W, Irvin P, Oh S H, Levy J and Eom C-B 2021 *Sci. Adv.* **7** eabh1284

[194] Nagarajan V, Roytburd A, Stanishevsky A, Prasertchoung S, Zhao T, Chen L, Melngailis J, Auciello O and Ramesh R 2003 *Nat. Mater.* **2** 43–47
[195] Jang H W *et al* 2008 *Appl. Phys. Lett.* **92** 2008–10
[196] Bakaul S R, Prokhorenko S, Zhang Q, Nahas Y, Hu Y, Petford-Long A, Bellaiche L and Valanoor N 2021 *Adv. Mater.* **33** 2105432
[197] Abel S *et al* 2019 *Nat. Mater.* **18** 42–47
[198] Le Bourdais D, Agnus G, Maroutian T, Pillard V, Aubert P, Bachelet R, Saint-Girons G, Vilquin B, Lefeuvre E and Lecoeur P 2015 *J. Appl. Phys.* **118** 124509
[199] Liu M, Howe B M, Grazulis L, Mahalingam K, Nan T, Sun N X and Brown G J 2013 *Adv. Mater.* **25** 4886–92
[200] Wang H, Shen L, Duan T, Ma C, Cao C, Jiang C, Lu X, Sun H and Liu M 2019 *ACS Appl. Mater. Interfaces* **11** 22677–83
[201] Shen L *et al* 2017 *Adv. Mater.* **29** 1702411
[202] Jin C, Zhu Y, Han W, Liu Q, Hu S, Ji Y, Xu Z, Hu S, Ye M and Chen L 2020 *Appl. Phys. Lett.* **117** 252902
[203] Guo J, Chen W, Chen H, Zhao Y, Dong F, Liu W and Zhang Y 2021 *Adv. Opt. Mater.* **9** 2002146
[204] Guzelturk B and Lindenberg A 2021 *MRS Bull.* **46** 704–10
[205] Ji Y, Wang D, Wang Y, Zhou Y, Xue D, Otsuka K, Wang Y and Ren X 2017 *npj Comput. Mater.* **3** 43
[206] Takenaka H, Grinberg I, Liu S and Rappe A M 2017 *Nature* **546** 391–5
[207] Sharma P A, Kim S B, Koo T Y, Guha S and Cheong S-W 2005 *Phys. Rev.* B **71** 224416
[208] Fernandez A, Kim J, Meyers D, Saremi S and Martin L W 2020 *Phys. Rev.* B **101** 094102
[209] Moya X, Kar-Narayan S and Mathur N D 2014 *Nat. Mater.* **13** 439–50
[210] Moya X *et al* 2020 *Science* **370** 797–803
[211] Zhang X X, Tejada J, Xin Y, Sun G F, Wong K W and Bohigas X 1996 *Appl. Phys. Lett.* **69** 3596–8
[212] Nair B, Usui T, Crossley S, Kurdi S, Guzmán-Verri G G, Moya X, Hirose S and Mathur N D 2019 *Nature* **575** 468–72
[213] Stern-Taulats E, Castán T, Mañosa L, Planes A, Mathur N D and Moya X 2018 *MRS Bull.* **43** 295–9
[214] Mahajan R, Chiu C-P and Chrysler G 2006 *Proc. IEEE* **94** 1476–85
[215] Moya X *et al* 2013 *Nat. Mater.* **12** 52–58
[216] Mischenko A S, Zhang Q, Scott J F, Whatmore R W and Mathur N D 2006 *Science* **311** 1270–1
[217] Pandya S, Wilbur J D, Bhatia B, Damodaran A R, Monachon C, Dasgupta A, King W P, Dames C and Martin L W 2017 *Phys. Rev. Appl.* **7** 034025
[218] Greppmair A, Galfe N, Amend K, Stutzmann M and Brandt M S 2019 *Rev. Sci. Instrum.* **90** 044903
[219] Vales-Castro P *et al* 2021 *Phys. Rev.* B **103** 054112
[220] Schick C *et al* 2016 *Fast Scanning Calorimetry* (Cham: Springer International Publishing)
[221] Šiškins M, Lee M, Mañas-Valero S, Coronado E, Blanter Y M, van der Zant H S J and Steeneken P G 2020 *Nat. Commun.* **11** 2698
[222] Liu Y, Infante I C, Lou X, Bellaiche L, Scott J F and Dkhil B 2014 *Adv. Mater.* **26** 6132–7
[223] Lisenkov S, Mani B K, Cuozzo J and Ponomareva I 2016 *Phys. Rev.* B **93** 064108
[224] Ikeda M S *et al* 2019 *Rev. Sci. Instrum.* **90** 083902
[225] Khassaf H, Patel T, Hebert R J and Alpay S P 2018 *J. Appl. Phys.* **123** 024102
[226] Pandya S, Velarde G, Zhang L, Wilbur J D, Smith A, Hanrahan B, Dames C and Martin L W 2019 *NPG Asia Mater.* **11** 26
[227] Velarde G, Pandya S, Karthik J, Pesquera D and Martin L W 2021 *APL Mater.* **9** 010702
[228] Moalla R, Vilquin B, Saint-Girons G, Le Rhun G, Defay E, Sebald G, Baboux N and Bachelet R 2017 *Nano Energy* **41** 43–48
[229] Karthik J, Agar J C, Damodaran A R and Martin L W 2012 *Phys. Rev. Lett.* **109** 257602
[230] Ivry Y, Lyahovitskaya V, Zon I, Lubomirsky I, Wachtel E and Roytburd A L 2007 *Appl. Phys. Lett.* **90** 172905
[231] Hopkins P E, Adamo C, Ye L, Huey B D, Lee S R, Schlom D G and Ihlefeld J F 2013 *Appl. Phys. Lett.* **102** 121903
[232] Liu C, Chen Y and Dames C 2019 *Phys. Rev. Appl.* **11** 044002
[233] Wang L and Li B 2007 *Phys. Rev. Lett.* **99** 177208
[234] Ihlefeld J F, Foley B M, Scrymgeour D A, Michael J R, McKenzie B B, Medlin D L, Wallace M, Trolier-McKinstry S and Hopkins P E 2015 *Nano Lett.* **15** 1791–5
[235] Ning S, Huberman S C, Zhang C, Zhang Z, Chen G and Ross C A 2017 *Phys. Rev. Appl.* **8** 054049
[236] Zheng M and Zheng R-K 2016 *Phys. Rev. Appl.* **5** 044002
[237] Langenberg E *et al* 2019 *Nano Lett.* **19** 7901–7
[238] Foley B M, Wallace M, Gaskins J T, Paisley E A, Johnson-Wilke R L, Kim J-W, Ryan P J, Trolier-McKinstry S, Hopkins P E and Ihlefeld J F 2018 *ACS Appl. Mater. Interfaces* **10** 25493–501
[239] Sandell S, Chávez-Ángel E, El Sachat A, He J, Sotomayor Torres C M and Maire J 2020 *J. Appl. Phys.* **128** 131101
[240] Nova T F, Disa A S, Fechner M and Cavalleri A 2019 *Science* **1079** 1075–9
[241] Nicoletti D, Casandruc E, Laplace Y, Khanna V, Hunt C R, Kaiser S, Dhesi S S, Gu G D, Hill J P and Cavalleri A 2014 *Phys. Rev.* B **90** 100503
[242] Disa A S, Nova T F and Cavalleri A 2021 *Nat. Phys.* **17** 1087–92
[243] Latini S, Shin D, Sato S A, Schäfer C, De Giovannini U, Hübener H and Rubio A 2021 *Proc. Natl Acad. Sci.* **118** e2105618118
[244] Bazzan M and Sada C 2015 *Appl. Phys. Rev.* **2** 040603
[245] Alibart O, D'Auria V, Micheli M D, Doutre F, Kaiser F, Labonté L, Lunghi T, Picholle É and Tanzilli S 2016 *J. Opt.* **18** 104001
[246] Yang J, Tang J, Ghasemian M B, Mayyas M, Yu Q V, Li L H and Kalantar-Zadeh K 2022 *ACS Photonics* **9** 905–13
[247] Juraschek D M and Narang P 2021 *Nano Lett.* **21** 5098–104
[248] Lahneman D J and Qazilbash M M 2021 *Phys. Rev.* B **104** 235433
[249] Bouras M, Han D, Cueff S, Bachelet R and Saint-Girons G 2019 *ACS Photonics* **6** 1755–62
[250] Suntivich J, May K J, Gasteiger H A, Goodenough J B and Shao-Horn Y 2011 *Science* **334** 1383–5
[251] Eom C J, Kuo D-Y, Adamo C, Moon E J, May S J, Crumlin E J, Schlom D G and Suntivich J 2018 *Nat. Commun.* **9** 4034
[252] Fernandez A, Caretta L, Das S, Klewe C, Lou D, Parsonnet E, Gao R, Luo A, Shafer P and Martin L W 2021 *Adv. Energy Mater.* **11** 2102175
[253] Wang J L, Gaillard F, Pancotti A, Gautier B, Niu G, Vilquin B, Pillard V, Rodrigues G L M P and Barrett N 2012 *J. Phys. Chem.* C **116** 21802–9
[254] Domingo N, Pach E, Cordero-Edwards K, Pérez-Dieste V, Escudero C and Verdaguer A 2019 *Phys. Chem. Chem. Phys.* **21** 4920–30
[255] Domingo N, Gaponenko I, Cordero-Edwards K, Stucki N, Pérez-Dieste V, Escudero C, Pach E, Verdaguer A and Paruch P 2019 *Nanoscale* **11** 17920–30

[256] Akhade S A and Kitchin J R 2012 *J. Chem. Phys.* **137** 084703
[257] Liu H, Qi J, Xu H, Li J, Wang F, Zhang Y, Feng M and Lü W 2022 *ACS Catal.* **12** 4119–24
[258] Manca N, Mattoni G, Pelassa M, Venstra W J, van der Zant H S J and Caviglia A D 2019 *ACS Appl. Mater. Interfaces* **11** 44438–43
[259] Lu Y-H *et al* 2020 *Nano Lett.* **20** 6364–71
[260] Lee M *et al* 2022 *Nano Lett.* **22** 1475–82
[261] Bistritzer R and MacDonald A H 2011 *Proc. Natl Acad. Sci. USA* **108** 12233–7
[262] Chen X *et al* 2020 *Nat. Phys.* **16** 631–5
[263] Burian M, Pedrini B F, Ortiz Hernandez N, Ueda H, Vaz C A F, Caputo M, Radovic M and Staub U 2021 *Phys. Rev. Res.* **3** 013225
[264] Can O, Tummuru T, Day R P, Elfimov I, Damascelli A and Franz M 2021 *Nat. Phys.* **17** 519–24